
Paleoceanography of northeastern Fram Strait since the last glacial maximum: Palynological evidence of large amplitude changes

Falardeau Jade ^{1,*}, De Vernal Anne ¹, Spielhagen Robert F. ^{2,3}

¹ GEOTOP UQAM, CP 8888, Montreal, PQ H3C 3P8, Canada.

² GEOMAR Helmholtz Ctr Ocean Res, D-24148 Kiel, Germany.

³ Acad Sci Humanities & Literature, D-55131 Mainz, Germany.

* Corresponding author : Jade Falardeau, email address : falardeau.jade@courrier.uqam.ca

Abstract :

Sea-surface conditions in northeastern Fram Strait since the last glacial maximum (LGM) were reconstructed from cores MSM5/5-712-2 and PS2863/1-2 based on palynological assemblages, ecological preferences of dinocysts and application of the modern analog technique. Dinocyst in LGM sediments are sparse, but their assemblages reflect mild summer conditions. Given the regional context and evidence from other tracers, the dinocyst assemblages of the LGM could relate to regional fluxes of dinocysts during exceptional mild summers. From 19 to 14.7 ka, dinocyst data suggest very cold conditions with extensive sea-ice cover, while abundant reworked palynomorphs indicate intense glacial erosion. An abrupt transition at 14.7-14.5 ka was marked by a peak in summer temperatures coinciding with a rapidly deposited sediment layer related to a regional meltwater plume event in western Svalbard. From 14.7 to 12.6 ka, large seasonal temperature contrasts with mild summers and cold winters together with low salinity indicate continuous melting of the Svalbard Barents Sea ice sheet fostered by warm climate. At 12.6 ka, the regional onset of the Younger Dryas was marked by cooling and increased salinity. On a regional scale, the 12.6-12 ka interval corresponds to an important transition involving enhanced circulation of Arctic waters around Svalbard and establishment of coastal fronts along its northern and western margins. Modern-like oceanic conditions with relatively high salinity and low seasonal temperature contrast developed at about 7.6 ka. Since then, a slight cooling is observed, especially in winter. This study offers a comprehensive picture of the deglacial phases in eastern Fram Strait with unique data on the sea-surface salinity, which controls surface water stratification and plays an important role in ocean circulation.

Keywords : Fram strait, Last glacial maximum (LGM), Late and post-glacial, Holocene, Temperature, Salinity, Sea ice, Dinocysts

1 **1. Introduction**

2

3 The Norwegian Atlantic Current and its northernmost derivatives reach the Arctic
4 Ocean notably through the Fram Strait, which is the main gateway between the
5 Atlantic and the Arctic oceans (Fahrbach et al., 2001; Maslowski et al., 2004;
6 Schauer, 2004). Hence, these currents are an important heat source to the Arctic
7 Ocean shaping the northern limit of the regional sea-ice margins, which in turn plays
8 an important role for the energy budget at the Earth's surface. Furthermore, as the
9 Atlantic Water (AW) flows northward in eastern Fram Strait, heat loss to the
10 atmosphere accompanied with surface water cooling leads to increased density of
11 surface waters, thus potentially contributing to both the strength of the Atlantic
12 Meridional Overturning Circulation (AMOC) and the rate of North Atlantic Deep
13 Water (NADW) formation. Therefore, the oceanography of the Fram Strait is critical
14 not only for the climate in the Arctic realm but also for the global thermohaline
15 circulation. In this context, the objective of the present study is to document changes
16 in sea-surface conditions in the northeastern Fram Strait since the Last Glacial
17 Maximum (LGM; 23-19 ka; Kucera et al., 2005) to assess the role of northward heat
18 flux from AW advection on deglaciation and climate variations during the
19 postglacial.

20

21 Many studies have investigated the changes in AW inflows in Fram Strait during the
22 LGM and the deglaciation. Most of them are based on planktic and/or benthic
23 foraminifer assemblages and stable isotope analyses of foraminifer shells (cf.
24 Hebbeln et al., 1994; Sarnthein et al., 1995, 2003; Nørgaard-Pedersen et al., 2003;
25 Hald et al., 2001, 2007; Ślubowska-Woldengen et al., 2007, 2008; Rasmussen et al.,
26 2007, 2012; Werner et al., 2011, 2013, 2016; Aagaard-Sørensen et al., 2014a-b,
27 Chauhan et al., 2014; Zamelczyck et al., 2014; Bartels et al., 2017; Consolaro et al.,

28 2018). Other studies are based on sedimentological data (Andersen et al., 1996;
29 Forwick and Vorren, 2009; Jessen et al., 2010). However, as most of these studies
30 document paleoceanographical conditions in sub-surface and bottom waters, there is
31 still little information on the surface water conditions. To date, reconstructions of past
32 sea-surface conditions mostly document sea-ice cover using the organic biomarker
33 IP₂₅ (Müller et al., 2012; Müller and Stein, 2014; Bartels et al., 2017) and sea-surface
34 temperature estimated from alkenones during the LGM (Rosell-Melé and Comes,
35 1999) and the Early Holocene (Calvo et al., 2002; Marchal et al., 2002;
36 Risebrobakken et al., 2011). Data documenting variations of seasonal temperatures
37 and sea-surface salinity off western Svalbard since the LGM remain rare.

38

39 Here we present two new dinoflagellate cyst (or dinocyst) records from northeastern
40 Fram Strait covering the last 23,000 years. The data were used to apply the modern
41 analog technique for quantitative reconstruction of several sea-surface parameters,
42 including winter and summer sea-surface temperatures (SSTs) and sea-surface
43 salinities (SSSs), along with sea-ice cover extent (month/yr) and productivity
44 (gC/cm²yr), simultaneously. Hence, our data provide information on freshwater
45 inputs from glaciers and seasonal gradients of temperatures (Rochon et al., 1999; de
46 Vernal et al., 2001, 2005, 2013; Grøsfjeld et al., 2009), which are critical parameters
47 in ice-ocean dynamics, especially during phases of ice retreat. Core sites MSM5/5-
48 712 and PS2863 are located on the western and northwestern continental slopes of
49 Svalbard (Fig. 1; Table 1). Previous studies from site MSM5/5-712 (Spielhagen et al.,
50 2011; Werner et al., 2013; Aagaard-Sørensen et al., 2014a; Zamelczyk et al., 2014)
51 have provided a stratigraphic framework with multidecadal temporal resolution in
52 which biomarkers and stable isotopes have illustrated qualitatively changes of the
53 AW inflow and sea-ice cover extent (Werner et al., 2011, 2013; Müller et al., 2012;
54 Müller and Stein, 2014; Spielhagen et al., 2014; Zamelczyk et al., 2014). In addition

55 to developing a more detailed portrait of the surface water conditions from the LGM
56 to present, our study of the two above mentioned sites aims at contributing to a better
57 understanding of the AW modifications along its pathway, from the relatively
58 confined channel of the eastern Fram Strait to the open Arctic Ocean north of
59 Svalbard, where strong ocean-atmosphere heat transfer presently occurs.

60

61 **2. Regional hydrography**

62

63 There are two main currents in the Fram Strait (Fig. 1; Fahrbach et al., 2001; Schauer,
64 2004; Rudels et al., 2005; Schauer et al., 2008). In the west, the East Greenland
65 Current (EGC) flows southward and transports cold and fresh waters from the Arctic
66 Ocean, thus playing a major role in iceberg and sea-ice export to the North Atlantic.
67 In the east, the West Spitsbergen Current (WSC) circulates northward along the
68 western continental slope of Svalbard and carries relatively warm and saline Atlantic
69 waters towards the Arctic Ocean. It originates from two distinct branches in the
70 Nordic Seas: the Norwegian Atlantic Slope Current (NwASC) and the Norwegian
71 Atlantic Current (NwAC), further named the WSC western branch. Parts of the
72 NwASC turns east at the surface into the shallow Barents Sea (Rudels et al., 1999),
73 where it is responsible for significant heat transport (5.07 Sv; 106 TW; Maslowski et
74 al., 2004) while the rest of the water masses continues north as the WSC core. Parts
75 of the WSC western branch bifurcate to the west without extending further than 80-
76 81°N (Rudels et al., 2000) through the Return Atlantic Current (RAC) following
77 topographical features, to finally turn south with the EGC (Gascard et al., 1995). The
78 two main branches converge into the WSC core around 78°N due to the bottom
79 topography (Walczowski and Piechura, 2007).

80

81 Because of the complex bathymetry of the Fram Strait, the WSC core splits into three
82 branches (Manley, 1995): a western branch (RAC), a central branch called the
83 Yermak Branch (YB), which flows north and reaches the Arctic Ocean along the
84 western and northern shelf of the Yermak Plateau (YP), and the Svalbard Branch
85 (SB). This branch flows east following the northern Svalbard shelf and continues by
86 circulating south of the Yermak Plateau.

87

88 Arctic waters circulate southward through the East Spitsbergen Current (ESC) and
89 follow the east Svalbard coast in the Barents Sea (Loeng, 1991). The ESC is renamed
90 as the South Cape Current (SCC) after passing the Storfjorden, in south Svalbard, and
91 follows the western coast of Svalbard carrying freshwater from glaciers melt and
92 river runoff in summer (Skogseth et al., 2005).

93

94 The WSC transports about 11.6 Sv at 78°50'N corresponding to 70.6 TW of heat
95 (Walczowski et al., 2005). Previous studies from moored instruments obtained
96 similar values with mean annual transport of 9 ± 2 to 10 ± 1 Sv (Schauer, 2004) and a
97 monthly mean average of 9.5 ± 1.4 Sv (Fahrbach et al., 2001). The regional sea-ice
98 cover extent is mainly controlled by the advection of warm AW. Site MSM5/5-712 is
99 located under the path of the WSC on the western continental slope of Svalbard and it
100 is therefore largely influenced by AW. Site PS2863 is located 200 km north of
101 MSM5/5-712 downstream of the WSC and is thus under distal influence of AW and
102 close to the limit of mean sea-ice extent in summer which corresponds to the Polar
103 Front.

104

105 At site PS2863, the mean sea-surface temperature and salinity in summer are $2.3 \pm$
106 2.3°C and 33.3 ± 0.9 psu, respectively (1900-2001 data from the World Ocean Atlas
107 2001; Conkright et al., 2002; Table 1). The sea-ice cover is highly variable at the core

108 site since it is located close to the sea-ice margin. Hence, the sea-ice cover with
109 concentration > 50% varied between 0 and 11 months/yr from 1954 to 2003, with an
110 average of 3.7 ± 3.2 months/yr (data provided by the National Snow and Ice Data
111 Center -NSIDC- in Boulder). At site MSM5/5-712, the mean-sea surface temperature
112 and salinity in summer are 4.9 ± 1.40 °C and 34.73 ± 0.43 psu, respectively
113 (Conkright et al., 2002; Table 1). Sea-ice cover with concentration > 50% varied
114 between 0 and 6 months/yr from 1954 to 2003, with an average of 1.2 ± 1.7
115 months/yr (data from NSIDC, 2003).

116

117 **3. Methods**

118

119 Gravity core PS2863-1 (80°33.46'N, 10°17.96'E; water depth 808 m) was collected in
120 1997 during the *RV Polarstern* expedition ARK-XIII/2 (Stein and Fahl, 1997). The
121 core is 580 cm long. The uppermost 184 cm were subsampled at 4 cm intervals for
122 palynological analyses. Box core PS2863-2 from the same location is 41 cm long. It
123 was subsampled at a 1 cm resolution (Table 1). The results from the two cores were
124 combined into a composite record referred to as PS2863 (see detailed counts of
125 palynomorphs in Falardeau, 2017).

126

127 Sediment core MSM5/5-712-2 (78°54.94'N, 6°46.04'E; water depth 1487 m) was
128 retrieved from *RV Maria S. Merian* in 2007 (Budéus, 2007). The kastenlot core has a
129 total length of 950 cm. Palynological results from this core (hereafter MSM5-712) are
130 presented at 4 cm intervals for the uppermost 283 cm and at 8 cm intervals down to
131 777 cm (Table 1).

132

133 Samples were prepared for palynological analyses in the micropaleontology
134 laboratory of GEOTOP according to standard procedures (de Vernal et al., 2010). In

135 short, approximately 5 cc of sediment were wet sieved at 10 and 106 μm after
 136 measurement of their volume and their weight (wet and dry). One capsule of
 137 *Lycopodium clavatum* with a known number of spores was added for further
 138 palynomorph concentration calculations (Matthews, 1969). The 10-106 μm fraction
 139 was treated with hydrochloric acid (HCl 10%) and hydrofluoric acid (HF 49%) to
 140 dissolve carbonate and silica particles, respectively. Residues were mounted on slides
 141 in glycerin jelly for microscopic analysis.

142 Dinocyst and other palynomorph concentrations were calculated as follows:

$$N_p = (N_e \times n_p) / n_e$$

143 where N_p is the total number of dinocysts in the sample, N_e is the known number of
 144 *L. clavatum* spores in the capsule added to the sample, n_p is the number of dinocysts
 145 counted and n_e is the number of *L. clavatum* counted. The total number of dinocysts
 146 was used to calculate dinocyst concentrations as follows:

$$N_p / \text{dry sediment weight (g)} = \text{Dinocyst concentrations (\#/g)}$$

147 or:

$$N_p / \text{volume (cm}^3\text{)} = \text{Dinocyst concentrations (\#/cm}^3\text{)}$$

148 The total uncertainty of calculated concentration was calculated from the equation of
 149 Stockmarr (1971), which is based on the standard deviation of number of spores in
 150 the *L. clavatum* capsules, the error on the number of cysts counted and number of *L.*
 151 *clavatum* spores counted. The total error never exceeded 22%.

152

153 The results from the latter calculation for dinocyst concentrations was used to
 154 determine the fluxes:

$$\text{Sedimentation rate (cm/yr)} \times \text{Concentration (\#/cm}^3\text{)} = \text{Flux (\#/cm}^2\text{/yr)}$$

155 The sedimentation rate was calculated from a linear interpolation between each
 156 sample based on the established age vs. depth relationship (see text section 4, Fig. 2).

157

158 Analysis of the palynological content includes dinoflagellate cysts, foraminiferal
159 organic linings, the freshwater chlorophyte *Pediastrum* and reworked pre-Quaternary
160 palynomorphs. The foraminiferal linings, consisting of refractory organic matter, can
161 be used as indirect tracers of productivity as benthic foraminifers depend upon
162 organic matter fluxes (e.g., de Vernal et al., 1992; Leduc, 2001; Jorissen et al., 2007).
163 Pollen grains, spores and other palynomorphs were also counted (see Falardeau,
164 2017), but not used here.

165

166 Dinocyst species were identified using the standardized taxonomy and nomenclature
167 of Rochon et al. (1999). On average, 318 dinocysts were counted per sample except
168 in the LGM samples (110 specimens on average) which are characterized by low
169 concentrations. Dinocyst counts range from a minimum of 27 specimens at site
170 PS2863 (LGM sample) to a maximum of 693 specimens counted in a late Holocene
171 sample of site MSM5-712.

172

173 Reworked palynomorphs which result from the erosion of older sedimentary rocks
174 and subsequent deposition (Streel and Bless, 1980) include pollen grains, spores,
175 acritarchs as well as dinocysts. They were distinguished by a darker color and a
176 flattened morphology owing to the longer preservation period in the sediment. A
177 number of well-preserved palynomorphs identified at genus or family level to be
178 stratigraphically older than Quaternary were also counted as reworked (cf. Williams
179 and Brideaux, 1975). For example, specimens of the dinocyst *Wetzeliella* were
180 identified and are stratigraphically associated with the Mid-Oligocene. When the
181 source was terrigenous, reworked palynomorphs could be significantly older like
182 *Neoraistrickia* and *Cicatricosisporites* which are pteridophyte spores from the
183 Cretaceous.

184

185 Quantitative reconstructions of sea-surface parameters were made using the modern
186 analog technique (MAT; Guiot, 1990), which was applied to the dinocyst
187 assemblages. Although the MAT has been criticized as it possibly underestimates the
188 error of prediction due to spatial autocorrelation (Telford, 2006; Telford and Birks,
189 2006), this approach remains more appropriate than calibration techniques for
190 dinocyst-based reconstructions of sea-surface conditions and foraminifer-based
191 reconstructions of sea-surface temperatures (e.g., Guiot and de Vernal, 2011). Here,
192 we applied MAT following the procedure described by de Vernal et al. (2013). We
193 have calculated the most probable values from a set of 5 analogs identified in the
194 reference dinocyst database which includes data from the Greenland margins (cf.
195 Allan et al., 2018) in addition to data from the n = 1492 database (de Vernal et al.,
196 2013) for a total of 1776 sites. The procedure consists of log-transformation of the
197 occurrence (per mil) of 66 dinocyst taxa. The distance between modern and fossil
198 spectra (sum of the differences in taxa occurrence expressed in log values) allows
199 identifying the 5 best analogs. The most probable sea-surface values correspond to
200 the average of the selected analogs, weighted inversely to the distance. Poor analogs
201 having a distance larger than a threshold value of 1.2 are excluded from the
202 reconstructions. The uncertainty of sea-surface reconstructions or the error of
203 prediction calculated from a subset (1/6) of the data base are established at $\pm 1.3^{\circ}\text{C}$
204 and $\pm 1.6^{\circ}\text{C}$ for the sea-surface temperatures in winter and summer respectively, \pm
205 2.1 psu for the salinity in summer and ± 1.3 month/yr for the sea-ice cover (cf. Allan
206 et al., 2018). The error of prediction is large for salinity due to the high variability in
207 the low salinity domain. When considering only the > 30 psu salinity range, the
208 uncertainty is ± 0.63 psu.

209

210 **4. Chronology**

211

212 The chronology of core MSM5-712 (Table 2; Fig. 2) is based on 18 accelerator mass
213 spectrometry (AMS) ^{14}C dates obtained from planktic foraminifers
214 (*Neogloboquadrina pachyderma*) and compiled by Müller et al. (2012) and Müller
215 and Stein (2014). Additional age tie points were obtained from correlations with the
216 total organic carbon content of PS2837-5 (Nørgaard-Pedersen et al., 2003) and the
217 western Svalbard reference stratigraphy of Jessen et al. (2010) (for details see Müller
218 and Stein, 2014). A distinct interval of rapid sedimentation rate is well represented in
219 core MSM5-712 between 657 and 433 cm.

220

221 The chronology of core PS2863-1 is based on five AMS ^{14}C dates on *N. pachyderma*
222 (Table 2; Fig. 2). In addition, a sixth chronological tie point was obtained from
223 stratigraphic correlation with the nearby core PS2837-5 (81°13.99'N, 02°22.85'E; Fig.
224 1) from the western slope of the Yermak Plateau (Nørgaard-Pedersen et al., 2003). A
225 well-defined IRD peak with similar thickness and coarse fraction content in the
226 sediment sequence was found at 106.5 cm in core PS2863-1 and at 302.5 cm in core
227 PS2837-5 (Fig. 2). In core PS2837-5, the peak has an age of $14,202 \pm 285$ cal. years
228 BP, which was transferred to 106.5 cm in core PS2863-1. Further, a very fine grained
229 laminated layer at 133-120 cm in core PS2863-1 was associated with a regional
230 sedimentary event recorded all along the northwestern Barents Sea and the western
231 Svalbard continental slopes up to the Yermak Plateau (Jessen et al., 2010; Lucchi et
232 al., 2015). In Jessen et al. (2010), the interval started at $13,140 \pm 150$ ^{14}C years BP
233 and ended at $12,840 \pm 150$ ^{14}C years BP, which corresponds to $14,931 \pm 560$ and
234 $14,434 \pm 620$ cal. years BP, respectively. The rapidly deposited sediment in core
235 MSM5-712 occurs within the limits of the unit described by Jessen et al. (2010) with
236 a weighted mean age of 14,660-13,930 cal. years BP.

237

238 The age-depth relationship of cores PS2863-1, MSM5-712 and PS2837-5 was
239 defined using the Bacon 2.2 software based on Bayesian statistics with default
240 probability intervals of 95% (2-sigma) (Blaauw and Christen, 2011). All the original
241 and correlated AMS ^{14}C ages were calibrated using the Marine13 calibration curve of
242 Reimer et al. (2013) with an additional correction (δR) of 98 ± 37 years
243 calculated from six values from the Svalbard area (Olsson, 1980; Mangerud, 1972;
244 Mangerud and Gulliksen, 1975) of the Marine Reservoir Data Base of Calib 7.1
245 (<http://calib.org/marine/>). All ages in this study are given as thousand calibrated years
246 before present (ka), unless stated otherwise. We assumed that the surface of the cores
247 was modern with a possible error of 460 years for core PS2863-1 and 160 years for
248 core MSM5-712. Such errors were determined considering bioturbation in the upper
249 ~3.5 centimeters. In other words, the errors are equivalent to the projected age at 3.5
250 cm. The average sedimentation rate of the rapidly deposited layer found in both cores
251 is calculated to about 43 cm/kyr in core PS2863-1 and 309 cm/kyr in core MSM5-
252 712. With exception of this layer, the mean sedimentation rate in core PS2863-1 is
253 about 8 cm/kyr, which is much less than in core MSM5-712 characterized by mean
254 sedimentation rates of 27 cm/kyr.

255

256 **5. Results**

257

258 5.1 Palynological assemblages

259

260 Dinocysts largely dominate the palynological assemblages at both sites, MSM5-712
261 and PS2863, with concentrations recording similar positive trends towards present
262 (Fig. 3a, f). Prior to 17 ka, dinocyst concentrations were low (150-800 cysts/g in
263 MSM5-712 and 50-1000 cysts/g in PS2863). They were much higher after 17 ka (>
264 2000 cysts/g in MSM5-712 and > 1000 cysts/g in PS2863) with exception of a

265 marked minimum centered at 14.4 ka at site MSM5-712. The last 8000 years are
266 characterized by very high concentrations ranging 10^4 - 10^5 cysts/g, with a maximum
267 recorded in the upper part of the sequence representing the last 4000 years (Fig. 3a,
268 f). Site MSM5-712 records about twice as high cyst concentrations as site PS2863.
269 The concentrations led to calculated fluxes that are one order of magnitude higher in
270 the late and postglacial sediments of core MSM5-712 (~ 800 cysts/cm²/yr on the
271 average) than those of site PS2863 (~ 60 cysts/cm²/yr on the average) (Fig. 3b, g).
272 Beyond these general characteristics, a double concentration peak is recorded at
273 ~ 14.8 and ~ 13.9 ka in core MSM5-712 (Fig. 3f). Site PS2863 also recorded
274 maximum concentrations centered at 13.7 and 13 ka (Fig. 3a). However, the peaks are
275 less pronounced, possibly due to bioturbation and lower sedimentation rate at this
276 site.

277

278 The concentrations of benthic foraminifer linings are ranging from 100 to 2000
279 linings/g in sediments of the last 14 ka at site PS2863 (Fig. 3c, h). In core MSM5-
280 712, foraminifer lining concentrations continuously increased from 14 ka to present
281 (2500 linings/g on the average), mirroring the trend in dinocyst concentrations, which
282 both suggest a higher primary productivity after 14 ka and high organic carbon fluxes
283 especially during the Mid to Late Holocene (Fig. 3f, h). The concentrations of
284 reworked palynomorphs range from 500 to 2000/g, with highest values in the 20-12
285 ka interval (Fig. 3e, j). The *Pediastrum* counts are low in all samples (<30 specimens;
286 Falardeau, 2017) and their occurrence is thus reported as presence/absence (Fig. 3d,
287 i). At site PS2863, *Pediastrum* is generally present throughout the record, from 23 to
288 8 ka, while at site MSM5-712 three intervals of occurrence are distinguished at 23-17
289 ka, at 14.5-12 ka and at 9.5-8 ka. At both sites, *Pediastrum* is nearly absent after 8 ka
290 except three sparse occurrences at site MSM5-712 (Fig. 3d, i).

291

292 The dinocyst assemblages show high species diversity, with occurrences of both
293 phototrophic and heterotrophic taxa at the two sites (Fig. 4). Among the phototrophic
294 taxa, *Operculodinium centrocarpum*, *Nematosphaeropsis labyrinthus*,
295 *Bitectatodinium tepikiense*, *Spiniferites elongatus* and *Spiniferites ramosus* dominate
296 the assemblages, reaching more than 50% in some intervals. The accompanying taxa
297 comprised the cyst of *Pentapharsodinium dalei*, *Impagidinium pallidum* and
298 *Spiniferites* spp. (5-20%). Heterotrophic species are represented by *Brigantedinium*
299 spp. and *Islandinium minutum* with low abundance of *Islandinium cezare* and
300 *Selenopemphix quanta* (< 5%). Dinocysts are present throughout the record, including
301 heterotrophic taxa that are more sensitive to dissolution (cf. Kodrans-Nsiah et al.,
302 2008), suggesting generally good preservation of organic-walled microfossils in the
303 sediment. The dinocyst record is characterized by large variations in assemblages
304 since the LGM. The major transitions are generally synchronous at both sites and the
305 assemblages are similar, which allowed us to recognize five distinct dinocyst
306 assemblage zones at regional scale (Fig. 4).

307

308 In Zone V (~23-19 ka), the dinocyst assemblages are distinguished by abundant *B.*
309 *tepikiense* reaching up to 40% in PS2863 and 46% in MSM5-712. The occurrence of
310 this species is a characteristic feature of the LGM interval in the northern North
311 Atlantic (de Vernal et al., 2005). According to its modern distribution, *B. tepikiense*
312 tolerates high amplitude variations of seasonal temperature and relatively low salinity
313 in stratified surface waters (Rochon et al., 1999; de Vernal et al., 2001, 2005). The
314 occurrence of *O. centrocarpum*, which is a cosmopolitan species, is also high with a
315 relative abundance of about 30%. Three peaks of *Brigantedinium* spp. (33%, 53% and
316 20%) are observed, but only at site MSM5-712. The dinocyst assemblages in core
317 MSM5-712 also holds low but significant concentrations of more temperate species
318 such as *Spiniferites mirabilis* (< 3.5%) and *Lingulodinium machaerophorum* (< 5%).

319

320 Zone IV, which spans ~19 to 14.7 ka, is characterized by the dominance of
321 *Brigantedinium* spp. with relative abundance of 76-94% at site PS2863 and of 68-
322 87% at site MSM5-712. The accompanying taxa include *I. minutum*, *S. elongatus* and
323 *O. centrocarpum* (0-10%).

324

325 Zone III spans from 14.7 to 12.6 ka and covers most of the Bølling-Allerød
326 interstadial (BA; 14.7-12.9 ka; Rasmussen et al., 2006). The boundary between zones
327 III and IV corresponds to the base of the very high sedimentation rates layer. This
328 sedimentary transition is also characterized in both dinocyst records by a subtle
329 increase in *O. centrocarpum* and a more general increase of cysts from the genus
330 *Gonyaulax*, represented notably by *S. elongatus* at site PS2863 and by *B. tepikiense* at
331 site MSM5-712, together with a decrease of heterotrophic taxa (cf. *Brigantedinium*
332 spp.). Zone III is characterized by short-lived variations of high amplitude in the
333 dinocyst assemblages of both cores. It is also marked by some discrepancies between
334 the two records. In particular, dinocyst assemblages of site PS2863 are mainly
335 dominated by *Spiniferites* taxa, mostly *S. elongatus* from 14.7 to 13.7 ka and *S.*
336 *ramosus* from 13.7 to 12.6 ka. In this interval, the specimens of *S. ramosus* include
337 wide ranges of body size and shape, the length of processes and the presence/absence
338 of an apical boss. They also include specimens with processes joined by more or less
339 complete trabecula network, ranging from a typical *S. ramosus* to a
340 *Nematosphaeropsis*-like morphology (see text section 6.2.3, Fig. 5). At site MSM5-
341 712, the interval is characterized by a very short peak of *B. tepikiense* at 14.6-14.5 ka.
342 *Brigantedinium* spp. dominates the assemblages from 14.5 to 14.1 ka. It is
343 progressively replaced by *O. centrocarpum*, *S. elongatus*, *S. ramosus*, the cysts of *P.*
344 *dalei* and *I. minutum*. At 13.2-12.6 ka, *O. centrocarpum* increases by about 10% at
345 the expense of *S. ramosus*. Despite differences between the assemblages of Zone III,

346 the two sites are characterized by significant occurrences of different morphotypes of
347 *S. ramosus*.

348

349 Zone II covers the latest Pleistocene and the early Holocene (12.6-7.6 ka). It is
350 characterized by high relative abundance of *O. centrocarpum* and the first significant
351 occurrence of *I. pallidum*. Beyond these general features, there are differences in the
352 dinocyst assemblages of the two cores. While the dinocyst assemblages in core
353 MSM5-712 contain abundant heterotrophic taxa, especially *I. minutum* (10-50%) and
354 *Brigantedinium* spp. (5-30%), the dinocyst assemblages at site PS2863 are almost
355 entirely composed of phototrophic taxa such as *N. labyrinthus*, the cyst of *P. dalei*,
356 and *O. centrocarpum* (Fig. 4).

357

358 Finally, Zone I covers the interval from 7.6 ka to present. It is characterized by the
359 dominance of *O. centrocarpum*, which constitutes about 70% of the assemblages in
360 both cores. *N. labyrinthus* and *I. minutum* are the main accompanying taxa while *I.*
361 *pallidum* records about 3-9% at site PS2863 but does not exceed 2% at site MSM5-
362 712.

363

364 5.2 Reconstructions of sea-surface conditions

365

366 Application of MAT revealed close modern analogs, with 5 modern analogs used for
367 the reconstruction in all samples. Distances between modern analogs and fossil
368 assemblages are lower than 0.2 for most samples and never exceed the threshold
369 value of 1.2 (Figs. 6f, 8f). Therefore, the reconstructions are as reliable as possible for
370 most of the samples. Relatively large distances from modern analogs, however, are
371 recorded between ~23 and 19 ka (mean of 0.62 and of 0.61 in MSM5-712 and
372 PS2863, respectively), at ± 14.5 ka (mean of 0.46) and 10.7 ka (mean of 0.84) at site

373 MSM5-712 and between 17.1 and 16.6 ka at site PS2863 (mean of 0.50) (Figs. 6f,
374 8f). In these intervals, one must be more cautious with quantitative estimates.

375

376 The reconstruction of sea-surface conditions from the MAT is generally coherent at
377 the two sites (Fig. 9). From 23 to 7.6 ka, high amplitude changes of all parameters are
378 recorded with a distinctive higher frequency between 14.7 and 13 ka, especially in
379 core MSM5-712, whereas the establishment of more stable conditions similar to
380 present ones occurred after 7.6 ka.

381

382 In Zone V spanning ~23-19 ka, sea-surface conditions reconstructed from the MAT
383 point to a strong seasonality with high temperatures in summer (13-16.5°C), but low
384 temperatures in winter (1.7-1.9°C) (Fig. 9a). Summer salinity was relatively low with
385 a mean of 31.6 psu at site MSM5-712, but the mean was 1 psu higher at site PS2863
386 (Fig. 9b). Such conditions are compatible with estuarine and coastal environments,
387 where modern analog assemblages are characterized by *B. tepikiense*. The occurrence
388 of *Pediastrum* also indicates freshwater inputs (Figs. 6c, 8c). However, the
389 reconstructions indicate almost no sea-ice cover and relatively high primary
390 productivity (Figs. 6d-e, 8d-e), which can be challenged in the context of the LGM.
391 Hence, intervals of low phytoplankton productivity (Rosell-Melé and Comes, 1999;
392 Müller and Stein, 2014), as well as low dinocyst concentrations (de Vernal et al.,
393 2005, 2006) were reported from the Nordic Seas during the LGM, which is coherent
394 with the low dinocyst fluxes at the study sites (Fig. 3b, g).

395

396 Zone IV, from ~19 to 14.7 ka, corresponds to the coldest conditions of the entire
397 record with extensive sea-ice cover (5-10 months/yr) and summer SSTs of about 4-
398 5°C at both sites (Fig. 9a, c). During this interval, sea-surface salinity remained low,

399 of about 31.1 and 31.7 psu in summer, at sites PS2863 and MSM5-712, respectively
400 (Fig. 9b).

401

402 In Zone III, spanning 14.7-12.6 ka, the two sites yielded different results in the first
403 half of the zone (Fig. 9) as could be expected from the discrepancies in the dinocyst
404 assemblages. The sea-surface estimates from site PS2863 indicate a reduced sea-ice
405 cover extent (mean of 2.4 months/yr) and warmer summer conditions up to 12.3°C,
406 which corresponds to large seasonal contrasts of temperature (Fig. 8a, d). They also
407 point towards saltier surface waters with an increase of about 1 psu (Fig. 8b). The
408 estimates from core MSM5-712 suggest warm sea-surface conditions reaching about
409 12°C in summer, similar as in PS2863, and relatively low SSSs (Fig. 6a, b), which is
410 compatible with the occurrence of the *Pediastrum* related to freshwater inputs (Fig.
411 6c). The high temporal resolution of analyses in core MSM5-712 permitted to
412 identify two short-lived events of large amplitude. One occurred at ~14.7-14.5 ka and
413 corresponds to peaks of *B. tepikiense* and *O. centrocarpum*. The other occurred at
414 ~14.5-14.1 ka concomitantly with a maximum abundance peak of *Brigantedinium*
415 spp. (Fig. 7i, j, k). At 14.7 ka, a warm pulse is marked by summer SSTs up to 14.4°C
416 and 2 months/yr decrease in the sea-ice cover extent (Fig. 7a, e). In the first 100
417 years, the SSSs in summer were low with an average of 30.7 psu, but they increased
418 up to 33.4 psu between 14.6 and 14.5 ka (Fig. 7c). In the 14.5-14.1 ka interval, colder
419 conditions prevailed with enhanced sea-ice cover reaching a maximum of 9
420 months/yr (Fig. 7e). The SSTs drastically decrease down to 0.8°C, concomitantly
421 with a drop in primary productivity and dinocyst concentrations (Fig. 7a, g, h). The
422 SSSs remained relatively low with an average of 31.6 psu.

423

424 In Zone II, spanning 12.6 to 7.6 ka, summer SSTs decrease to a mean of 5.5-6°C at
425 both sites, which resulted in a reduced amplitude of seasonal temperatures (Fig. 9a).

426 The SSSs increased from 32.2 to 34.3 psu at site PS2863 and from 30.5 to 33.5 psu at
427 site MSM5-712 (Figs. 6b, 8b). The sea-ice cover increased to a maximum of 5
428 months/yr at 11.4 ka at site PS2863 and to an average of 7 months/yr at 11.9-10.7 ka
429 at site MSM5-712, prior to a decrease to 1-2 months/yr towards the end of the
430 interval (Figs. 6d, 8d).

431

432 In Zone I, corresponding to the last 7600 years, summer SSTs remained relatively
433 stable with values of about 4.5°C and 4.0°C at sites PS2863 and MSM5-712,
434 respectively (Fig. 9a). However, a decrease of about 1.5-2°C in winter SSTs and an
435 increase of 1-2 months/yr in sea-ice cover are recorded towards modern (Fig. 9a, c).
436 Estimated summer SSSs decrease by about 1 psu at site PS2863. A less pronounced
437 decrease of SSSs is recorded in core MSM5-712.

438

439 **6. Discussion**

440

441 6.1 The LGM Paradox

442

443 During the LGM, hydrographical conditions in the Nordic Seas were probably unique
444 with no perfect modern equivalent (cf. de Vernal et al., 2005, 2006; Figs. 6f, 8f). The
445 selected modern analogs of the LGM in our study cores were obtained from the
446 northeastern shore of the United States, the northern margin of Norway and the Gulf
447 of St. Lawrence where large amplitude seasonal gradients of temperature presently
448 prevail due to estuarine-type circulation. Such conditions do not exist in open ocean
449 settings such as Fram Strait today. Hence, the quantitative reconstructions of the
450 LGM must be interpreted with caution. In a context of low dinocyst concentrations,
451 there is also a risk of distortion of the signal due to distal input. However, this is

452 unlikely here considering the similarity of assemblages at both sites, MSM5-712 and
453 PS2863, which are located 200 km apart from each other.

454

455 Despite the low concentrations, the dominance of phototrophic taxa (Fig. 4) provides
456 evidence for open water conditions in eastern Fram Strait during the LGM, at least
457 episodically. This was previously inferred, not only from dinocysts (de Vernal et al.,
458 2000, 2005), but also from coccoliths (Hebbeln and Wefer, 1997; de Vernal et al.,
459 2000), alkenones (Rosell-Melé and Comes, 1999), IP₂₅ biomarkers (Müller and Stein,
460 2014; Xiao et al., 2015) and planktic foraminifers (Hebbeln et al., 1994; Sarnthein et
461 al., 1995, 2003; Weinelt et al., 1996, 2003; Nørgaard-Pedersen et al., 2003;
462 Pflaumann et al., 2003; Zamelczyk et al., 2014). Seasonally open water conditions
463 may even have prevailed along the northern continental slope of Svalbard, where high
464 fluxes of planktic and benthic foraminifers were recorded (Chauhan et al., 2014,
465 2016). Open waters, at least seasonally, in the Nordic Seas were probably an essential
466 moisture source for the rapid growth of the Svalbard Barents Sea ice sheet (SBSIS)
467 (Hebbeln et al., 1994). There is also ample evidence for strong subsurface inflow of
468 AW to the Nordic Seas, the Fram Strait and northern Svalbard during the LGM based
469 on planktic foraminifer concentrations and assemblages (Rørvik et al., 2013; Chauhan
470 et al., 2014, 2016), good calcium carbonate preservation (Zamelczyk et al., 2014) and
471 the $\delta^{18}\text{O}$ signals of planktic foraminifers (Nørgaard-Pedersen et al., 2003; Rasmussen
472 and Thomsen, 2008). Mg/Ca data in ostracods from the Arctic Ocean (Cronin et al.,
473 2012) also point to a strong inflow of AW, even warmer than at present, but probably
474 at a greater depth. The paleoceanographical records of the LGM are therefore
475 paradoxical as they may suggest relatively warm conditions in Fram Strait despite
476 generally cold climate.

477

478 The inflow of AW in the context of a heavily glaciated environment might have led to
479 high meltwater inputs and low surface salinity as indicated by the relative abundance
480 of *B. tepikiense* (Fig. 4). Stratified low density surface waters could have resulted in
481 low thermal inertia (low heat capacity). This would be coherent with the very large
482 amplitude of seasonal temperatures which were marked by freezing conditions in
483 winter and relatively warm summers (Fig. 9a). Despite uncertainties due to possible
484 reworking, alkenone data also suggest relatively warm sea-surface conditions in the
485 area (Rosell-Melé and Comes, 1999). A scenario of stratified surface water masses
486 during the LGM, which would have confined the AW at the subsurface, was
487 proposed by Bauch et al. (2001). However, in our dinocyst assemblages, the presence
488 of *O. centrocarpum* reflects phototrophic productivity in surface water and would
489 relate to AW (Rochon et al., 1999; Grøsfjeld et al., 2009), leading to hypothesize
490 advection of AW during the LGM. The paradoxically high summer SSTs during the
491 LGM might therefore be linked to low thermal inertia of the upper waters.
492 Alternatively, it may be related to occasional advection of AW at the surface.

493

494 A flow of AW near the surface, even occasional, and the relatively low salinity that
495 apparently prevailed throughout the LGM in the uppermost water layer are equivocal.
496 Since the percentages of *O. centrocarpum* are half of those recorded during the Mid-
497 Late Holocene (Fig. 4), surface conditions related to AW advection probably differed
498 from the modern situation and were possibly weakened or highly variable due to
499 freshwater discharges. De Vernal et al. (2006) proposed that sea-surface conditions in
500 the Nordic Seas were unstable during the LGM, with alternation of relatively warm
501 episodes due to strong northward AW fluxes and cold episodes with high meltwater
502 discharge and dense sea-ice cover. For instance, the dinocyst record of core MD95-
503 2010 in the southern Norwegian Sea pointed to very large amplitude centennial
504 variations of sea-surface conditions during the LGM, with oscillations between 0 to 6

505 months/yr of sea-ice cover and evidence of episodic high SSTs (cf. Eynaud et al.,
506 2004; de Vernal et al., 2006). The high-resolution record of Müller and Stein (2014)
507 also pointed to rapidly changing conditions from perennial to reduced sea-ice cover
508 (Fig. 10b) in response to perturbations in the advection of AW. Similarly, inflow of
509 relatively warm AW but unstable conditions in subsurface waters were reported from
510 foraminifer data (Rasmussen and Thomsen, 2008; Rørvik et al., 2013). Large
511 instabilities with rapid perturbations of AW advection might correspond to the
512 prompt response of the AMOC to iceberg discharges and pulses of meltwaters during
513 the LGM (Levine and Bigg, 2008). Unfortunately, the current temporal resolution of
514 our records in addition to uncertainties due to limited biogenic material in LGM
515 sediment from Fram Strait does not permit to clearly identify short-lived fluctuations
516 in SSSs.

517

518 A possibility to explain the dinocyst assemblages of the LGM could be a deposition
519 to the sea floor only during brief intervals of relatively warm conditions, thus
520 representing extremes instead of average conditions and resulting in a warm bias in
521 quantitative estimates. Such a hypothesis was previously put forward by Nørgaard-
522 Pedersen et al. (2003) and Weinelt et al. (2003). If correct, the low dinocyst
523 concentrations could relate to dinoflagellate populations and cyst fluxes to the sea
524 floor during phases of sea ice-free conditions while intervals characterized by
525 permanent sea-ice cover correspond to almost nonexistent phytoplankton productivity
526 as suggested from biomarker studies in core MSM5-712 by Müller and Stein (2014).
527 The low dinocyst concentrations in the LGM sediment would therefore be the result
528 of dilution of biogenic fluxes during brief episodes of productivity with barren
529 sediments accumulated under quasi-perennial sea-ice cover. Considering mean annual
530 fluxes of dinocysts (~ 50 cysts/cm²) at site PS2863 since 18.5 ka, we calculate that the
531 average dinocyst content in LGM sediment (~ 1 cyst/cm²/yr; Fig. 3b) represents

532 productivity 50 times lower or an equivalent productivity occurring only during
533 exceptional summers, most of the interval being otherwise characterized by perennial
534 sea ice and zero dinocyst flux. In the latter case, which is likely in our view, we may
535 calculate that sea ice-free conditions in northeastern Fram Strait occurred only a
536 couple of years per century during the LGM, possibly as polynyas opened by
537 katabatic winds from the SBSIS. However, higher temporal resolution is needed for a
538 clear demonstration and unequivocal assessment of inter-annual variability of sea-
539 surface conditions in eastern Fram Strait.

540

541 6.2 Transition from the LGM to the postglacial

542

543 6.2.1 The early deglaciation and Heinrich Stadial 1

544

545 The transition from Zone V to Zone IV at about 19 ka is characterized by an
546 important change in assemblages with the decrease of *O. centrocarpum* and the
547 augmentation of the heterotrophic taxa *Brigantedinium* spp. and *I. minutum*. It
548 corresponds to a change towards particularly cold conditions and dense sea-ice cover
549 (Fig. 9a, c; cf. Rochon et al., 1999; de Vernal et al., 2001, 2013), which is coherent
550 with a decrease in the percentages of subpolar species in planktic foraminifer
551 assemblages of the eastern Fram Strait during the same interval (Zamelczyk et al.,
552 2014). This transition occurred concomitantly with an increase of reworked
553 palynomorphs at both core sites (Fig. 3e, j) pointing to intense glacial erosion, which
554 closely followed the IRD signal recorded at 20.5 ± 0.5 ka on the western Svalbard
555 slope (Jessen et al., 2010). The cooling after ~19 ka probably occurred in an early
556 phase of the SBSIS deglaciation recorded at about 19-17 ka in the Fram Strait
557 (Hebbeln et al., 1994; Andersen et al., 1996; Landvik et al., 1998; Nørgaard-Pedersen
558 et al., 2003; Rasmussen et al., 2007). Decreased summer SST and enhanced sea-ice

559 cover extent after 19 ka were suggested to result from reduced AW inflows towards
560 the end of the LGM (Rasmussen et al., 2007). This is coherent with the lowest
561 relative abundance of *O. centrocarpum* (Fig. 4).

562

563 The low SSSs in both core records that characterize Zone IV (< 33 psu; Fig. 9b) and
564 the high concentrations of *Pediastrum* only at site PS2863 (Falardeau, 2017),
565 indicating a northern source of freshwaters, suggest large meltwater and iceberg
566 discharges from the SBSIS. Meltwater flow probably led to cold and buoyant surface
567 waters, which would be at the origin of the near shutdown of the AMOC at about 18-
568 17.5 ka (McManus et al., 2004; Hall et al., 2006; Stanford et al., 2011; see Fig. 10h)
569 and low $\delta^{18}\text{O}$ of planktic foraminifers in the Nordic Seas during the same interval
570 (Jones and Keigwin, 1988; Lehman et al., 1991; Hebbeln et al., 1994; Bauch et al.,
571 2001; Nørgaard-Pedersen et al., 2003; Rasmussen et al., 2007). Such a scenario
572 supports the hypothesis of Ivanovic et al. (2017) based on coupled model
573 experiments, which suggests that the acceleration of the Eurasian deglaciation at
574 ~18.5 ka and freshwater/meltwater delivered to the Arctic Ocean are at the origin of
575 the Heinrich Stadial 1 (H1). Hence, Zone IV would correspond to an interval that can
576 largely be associated with the H1 (Stern and Lisiecki, 2014). The reduced AMOC
577 strength and cooling in the northern North Atlantic would have preceded the
578 Laurentide Ice surge in Hudson Strait (e.g., Heinrich, 1988; Bond, 1993; Hemming,
579 2004), which has been dated from 17.9 to 15.7 ka in a detailed Labrador Sea record
580 (Gibb et al., 2014).

581

582 Consistent with our dinocyst assemblages, the $P_{\text{BIP}_{25}}$ data suggest dense sea-ice
583 coverage, but mostly from 19 to 17.5 ka (Müller and Stein, 2014; Fig. 10b). An
584 increase in primary productivity can be deduced from biomarker data after 17.5 ka
585 (Müller and Stein, 2014), which is synchronous with the increase in dinocyst

586 concentrations in both core records presented here (Fig. 3a, f). Generally, the shift at
587 17.5-17 ka suggests a transition from an extremely harsh environment during the
588 earliest phase of the deglaciation to more favorable and milder pelagic conditions,
589 which is in line with planktic foraminifer data from the Yermak Plateau (Chauhan et
590 al., 2014). The abrupt shift from a heavily glaciated environment to seasonal sea-ice
591 at that time, as deduced from the $P_{BIP_{25}}$ index (Müller and Stein, 2014), could
592 illustrate this change in primary producer conditions.

593

594 6.2.2 The rapidly-deposited detrital layer and Bølling-Allerød

595

596 At the base of Zone III, which is also marked by the rapidly deposited sediment layer,
597 there is a peak of high summer SSTs accompanied by reduced sea-ice cover (Fig. 7a,
598 e). This warm event is observed in core MSM5-712, probably because of the high
599 temporal resolution of analyses that permits to identify short-lived events. The
600 transition from Zone IV to III, characterized by increase in *O. centrocarpum*,
601 probably corresponds to enhanced AW contribution (Fig. 7j). It occurred near-
602 synchronously with the resumption of the AMOC at about 14.6 ka, coincident with
603 the BA warming (McManus et al., 2004; Stanford et al., 2011; see Fig. 10h).
604 Enhanced AW contribution probably led to regional warming, glacier retreat,
605 meltwater inputs and low salinity as suggested by the excursions of *B. tepikiense*
606 (Fig. 7i), the recurrence of the *Pediastrum* (Fig.6c) and minima in $\delta^{18}O$ recorded in *N.*
607 *pachyderma* shells from core MD95-2010 (Dokken and Jansen, 1999; see Fig. 7b). At
608 that time, benthic foraminifer assemblages indicate a shift from polar to subarctic
609 conditions along the western Svalbard margin (Ślubowska-Woldengen et al., 2007,
610 2008).

611

612 At 14.5 to 14.1 ka, shortly after the warm interval, our sea-surface reconstructions
613 indicate a completely reversed trend, with the recurrence of *Brigantedinium* spp. (Fig.
614 7k) and the onset of extremely cold conditions with extensive sea-ice cover (Fig. 7a,
615 e). This cold event covers the larger part of the rapidly deposited layer, which was
616 dated of 14,700 to 13,900 cal. years BP in core MSM5-712. This layer is probably the
617 same as the one on the upper continental slope of the Storfjorden identified by Lucchi
618 et al. (2015). It bears sedimentological features similar as those of the deposit
619 described by Jessen et al. (2010) from the western Svalbard and the Yermak Plateau
620 continental slopes. Hence, this sedimentological event might be of high significance
621 in the deglacial history of the SBSIS as it would originate from the scouring of the
622 northwestern Barents Sea continental shelf in response to a major ice sheet collapse
623 (Lucchi et al., 2015). The timing of such a collapse is coherent with the SBSIS limit
624 of Hughes et al. (2016), showing that the ice sheet extending to the central Barents
625 Sea and Bjørnjøya retreated between 15 and 14 ka. The rapid ice collapse might have
626 been triggered by the enhanced AW advection and related warming of surface water
627 as documented above, together with a eustatic sea level rise. The palynological
628 content of the rapidly deposited layer at both sites is characterized by a maximum in
629 reworked palynomorphs (Fig. 3e, j), implying erosional processes on the shelves and
630 subsequent outwash deposition. Our data thus suggest that this layer was formed from
631 the erosion and deposition of sediments originating from the northwestern Barents
632 Sea continental shelf. Furthermore, the occurrence of thermophilic and diversified
633 dinocyst assemblages at the very base of the rapidly deposited layer supports the
634 hypothesis of a warm pulse at the onset of the sedimentological event that has marked
635 the continental margins on a regional scale.

636

637 The low dinocyst concentrations (mean of 390 cysts/g) in sediments accumulated
638 from 14.5 to 14.3 ka (Fig. 7h) likely result from dilution with sediments from a

639 sediment-laden meltwater plume. Nevertheless, the calculated fluxes are about 140
640 cysts/cm²/yr during this interval, which corresponds to relatively high fluxes and
641 productivity.

642

643 From 14.1 to 12.6 ka (top of Zone III), recurring high SSTs possibly relate to
644 enhanced AW heat advection (Fig. 6a). However, while subpolar conditions are
645 recorded in bottom waters around Svalbard (Bartels et al., 2017), particularly between
646 14.5-13.5 ka (Ślubowska-Woldengen et al., 2007), the planktic foraminifer
647 assemblages rather indicate polar conditions during the BA interstadial (Rasmussen et
648 al., 2007; Aagaard-Sørensen et al., 2014b; Chauhan et al., 2014), probably linked to
649 heat loss to the atmosphere and/or outpouring of cold waters as suggested by
650 Rasmussen et al. (2007).

651 At the study sites, the SSTs are marked by high seasonal amplitudes from winter to
652 summer (Fig. 9a). Strong inflow of AW during the deglaciation probably initiated
653 atmospheric warming at the margin of the SBSIS and enhanced meltwater discharge,
654 leading to low salinities and a strong stratification of surface water. The low $\delta^{13}\text{C}$ of
655 *N. pachyderma* in core MSM5-712 throughout the BA also suggests stratification in
656 the water column (Aagaard-Sørensen et al., 2014b). Hence, the high SSTs in summer
657 can be ascribed to a low thermal inertia of the surface water layer together with heat
658 advection from AW. Enhanced ice calving and meltwater discharge during the
659 Allerød are indicated by coarse sediment and low $\delta^{18}\text{O}$ from foraminifer shells
660 (Andersen et al., 1996; Hald et al., 2001; Jessen et al., 2010; Zamelczyk et al., 2012;
661 Aagaard-Sørensen et al., 2014b, Bartels et al., 2017). The extensive sea-ice cover
662 reconstructed from the $P_{\text{BIP}_{25}}$ index during most of the BA was associated with
663 stratification related to meltwater discharge (Müller and Stein, 2014), which is
664 compatible with our interpretation.

665

666 The hypothesis of AW advection that would lead to enhanced meltwater inputs
667 during deglacial phases could explain the reverse relationship between the SSS and
668 the $\delta^{18}\text{O}$ at NGRIP during the Allerød period (Fig. 10i, j). In opposite situations, low
669 summer SSTs could suggest weakened inflow of AW, less stratified surface waters
670 with high thermal inertia or a vertical mixing of water masses. Therefore, in contrast
671 to intervals of high summer SSTs and large seasonal contrasts, the low summer SST
672 phases were not associated with pronounced SSS decreases during the deglaciation.

673

674 6.2.3 The *Spiniferites ramosus* morphotypes and sea-surface conditions at 14.1-
675 12.9 ka

676

677 The dinocyst assemblages of the Allerød interval (14.1-12.9 ka; Rasmussen et al.,
678 2006) are characterized by abundant specimens of *Spiniferites*, including the
679 cosmopolitan species *S. ramosus* (Fig. 4), and by the presence of a large variety of
680 morphotypes, ranging from typical *S. ramosus* to *Nematosphaeropsis*-like
681 morphologies (Fig. 5). This is particularly the case at ~13.4 ka where the highest
682 concentrations of *Spiniferites* are recorded, but other atypical specimens were
683 observed from 14.3 to 11.4 ka. The two dinocyst species *S. ramosus* and *N.*
684 *labyrinthus* are related to the same motile dinoflagellate species *Gonyaulax spinifera*
685 (Dodge, 1989). From culture experiments, Rochon et al. (2009) proposed that they
686 could be the two endmembers of the same genotype or at least related species.
687 According to Rochon et al. (2009), the different phenotypes only occur in salinities
688 between 25 and 30 psu, whereas typical *S. ramosus* and *N. labyrinthus* are usually
689 more abundant in saltier water of 32-36 psu and 31-37 psu, respectively (Rochon et
690 al., 1999; Marret and Zonneveld, 2003). Ellegaard (2000) also found unusual cyst
691 morphotypes more abundant during low salinity events in the last 2000 years in the
692 Limfjorden, northern Denmark. Other morphological disparities seem to be a

693 response to salinity constraints, like the processes length of *O. centrocarpum*
694 (Mertens et al., 2012) or the development of cross-shaped cysts in the Black Sea
695 during the Late Pleistocene (Rochon et al., 2002). From 14 to 12.6 ka, the analogs
696 selected for the MAT reconstructions are mainly from the Gulf of St. Lawrence.
697 However, analogs were also obtained from the Barents Sea off northern Norway and
698 the northeast shore of the United States. While all these analogs are associated with
699 warm summers ($> 8^{\circ}\text{C}$), they relate to variable salinities ranging from < 31 psu in the
700 Gulf of St. Lawrence to oceanic conditions at some other analog locations. In our
701 cores, the morphotypes occurred mostly in intervals of low reconstructed SSSs, with
702 exception of a few high-salinity excursions, notably at 13 ka (33.9 psu) at site PS2863
703 (Fig. 8b) and at 13.2 ka (32.4 psu) at site MSM5-712 (Fig. 6b). Hence, the interval
704 from 14 to 12.6 ka was apparently characterized by unstable conditions with high
705 amplitude variations of SSSs and large seasonal contrasts of temperatures, as it is
706 often the case in nearshore environments. The episode of strongly reduced SSSs we
707 calculate from core MSM5-712 at 14-12.6 ka coincides with accelerated glacial
708 retreat around Svalbard (e.g., Andersen et al., 1996; Hald et al., 2001). Hence,
709 morphological variations of processes during cyst formation may result from reduced
710 salinities as proposed by Rochon et al. (2009). Highly variable conditions and/or a
711 turbulent environment can also have impacted the cyst morphology.

712

713 6.2.4. The Younger Dryas interval

714

715 At the studied sites, the Younger Dryas interval (YD; 12.9-11.7 ka) as defined by
716 Rasmussen et al. (2006) corresponds to a transition from large regional meltwater
717 discharges resulting in low salinities of < 32 psu (Zone III) to modern-like
718 thermohaline properties in surface waters (Zone II; Fig. 9b). The occurrence of *I.*
719 *pallidum* at 12.5 ka marked this transition in the dinocyst assemblages at both sites,

720 especially at site PS2863 where it is more pronounced (Fig. 4). The first postglacial
721 occurrence of *I. pallidum* was reported by Matthiessen and Baumann (1997) at ~12.9
722 ka from core PS1295 (see Fig. 1). This taxon is a typical component of the modern
723 assemblages in the Nordic Seas and indicates cold ocean conditions (Matthiessen,
724 1995; Rochon et al., 1999; Grøsfjeld et al., 2009; Bonnet et al., 2010). A change in
725 the benthic fauna around Svalbard is also reported to have occurred at 12.5 ka as the
726 result of recurring cold bottom waters (Ślubowska-Woldengen et al., 2007, 2008).
727 The planktic foraminifer assemblages that continued to be dominated by *N.*
728 *pachyderma* during the BA also indicate cold conditions (Rasmussen, 2007; Aagaard-
729 Sørensen et al., 2014b). In surface waters, our data indicate a strong cooling with a
730 decrease of SSTs by about 10°C in summer (Fig. 9a). The cooling was accompanied
731 by an increase in SSSs, from 31 to 33 psu (Fig. 9b), which is probably related to
732 reduced meltwater discharges during a slowdown of the ice sheet retreat, as indicated
733 by a stabilization of the sea level (Landvik et al., 1987). The decrease in summer SST
734 was likely the result of a general cooling, but it could also be related in part to higher
735 thermal inertia in a more oceanic context marked by higher salinity due to lesser
736 meltwater discharges, weak stratification and deeper thermocline. More open ocean-
737 like conditions are coherent with the occurrence of *I. pallidum*, which is considered
738 oligotrophic, and are compatible with the multi-proxy paleoceanographic
739 reconstructions of northern Svalbard by Bartels et al. (2017). In our record, the sea-
740 ice cover extent started to increase at the onset of the YD and reached a maximum at
741 about 12.5 ka, which is almost coeval with a peak of $P_{BIP_{25}}$ (Müller and Stein, 2014;
742 Fig. 10a, b).

743

744 Although a cooling during the YD is generally assumed to have occurred at large
745 scale in the Northern Hemisphere (e.g., Alley, 2000; Andersen et al., 2004b; see Fig.
746 10j), the exact timing and the regional pattern of the climate signal in the Nordic Seas

747 and Svalbard area are not yet fully elucidated. Unlike in the Fennoscandian areas
748 (Stroeven et al., 2016), there is no evidence that local glaciers of western (Mangerud
749 and Landvik, 2007) and northern Svalbard (Bartels et al., 2017) experienced re-
750 advance during the YD. ^{10}Be data even revealed that the Linnébreen glacier on west
751 central Svalbard underwent a glacial retreat at that time (Reusche et al., 2014)
752 whereas extensive sea-ice cover likely prevailed off eastern Svalbard, in the
753 Storfjorden and the fjords of western Svalbard (Forwick and Vorren, 2009;
754 Kristensen et al., 2013; Rasmussen and Thomsen, 2014). Hence, the apparent offset
755 between southern vs. northern Fennoscandian glacier readvances during the YD can
756 be due to particularly cold and dry climate, which limited snow accumulation and
757 prevented glacier growth in the Svalbard area (cf. Mangerud and Landvik, 2007).

758

759 In the dinocyst assemblages of Zone II (12.6-7.6 ka), abundant *I. minutum*
760 characterized site MSM5-712 while maximum occurrence of the cyst of *P. dalei*
761 occurred at site PS2863 (Fig. 4). The discrepancies between the two sites are
762 probably due to local hydrographic conditions as this interval would correspond to
763 the development of the Arctic Coastal Front in western Svalbard and of the Polar
764 Front in northern Svalbard, respectively. The cyst of *P. dalei* has previously been
765 associated with the Polar Front, together with high productivity (Voronina et al.,
766 2001; Grøsfjeld et al., 2009). *I. minutum*, which is typical for sea-ice environments
767 and is often associated with a highly productive polynya (Hamel et al., 2002),
768 characterizes the modern surface Arctic waters around Svalbard (Grøsfjeld et al.,
769 2009). Therefore, from 12.6 to 7.6 ka, the study sites were probably in productive
770 zones close to the sea-ice margin. This is compatible with the development of coastal
771 fronts which was suggested to have occurred at 12.6 ka from the high concentration
772 of the benthic foraminifer *Nonionellina labradorica* in cores JM02-440 and NP94-51
773 (see Fig. 1; Koç et al., 2002; Ślubowska et al., 2005; Ślubowska-Woldengen et al.,

774 2007). Increased *N. labradorica* was also recorded at 12.7 ka on the northern margin
775 of Svalbard (Bartels et al., 2017). However, from a high relative abundance of *N.*
776 *labradorica*, Chauhan et al. (2014) defined the position of the Polar Front on the
777 southern Yermak Plateau near site PS2863 significantly earlier, at 14.4-11.5 ka. The
778 development coincides with an increase of *P. dalei* cyst numbers at site PS2863 prior
779 to its maximum abundance during Zone II (12.6-7.6 ka). Hence, the Polar Front
780 might have oscillated from a position close to site PS2863 northwest of Svalbard at
781 14.5-12.6 ka before it stabilized in a position close to the modern one (Fig. 1).

782

783 The establishment of the Arctic Coastal Front implies strengthened ESC and SCC.
784 Their influence on the Svalbard continental shelves, which could have accounted for
785 a cold and dry climate over Svalbard, are consistent with abundant *I. minutum*, an
786 indicator of Arctic waters in this context, and with sedimentological evidence of other
787 continental margin cores (Forwick and Vorren, 2009; Kristensen et al., 2013;
788 Rasmussen and Thomsen, 2014). It is also coherent with the near-synchronous
789 opening of the northeastern shelf of Svalbard at about 12.6 ka (Koç et al., 2002).
790 Open waters around Svalbard necessarily fostered Arctic water circulation through
791 the SCC and the ESC.

792

793 An increase in the strength of the EGC at about the same time, with enhanced
794 southward flow of Arctic waters through Fram Strait, was also inferred based on low
795 $\delta^{18}\text{O}$ in planktic foraminifers (Bauch et al., 2001; Zamelczyk et al., 2012) and the
796 radiogenic signature in sediments from core MC16 (cf. Hillaire-Marcel et al., 2013).
797 Regardless the precise timing of events, very important changes in sea-surface
798 circulation of Fram Strait and around Svalbard occurred during the YD. They were
799 likely related to a major reorganization of the ocean circulation in the Arctic and
800 subarctic Atlantic oceans. Enhanced export of freshwater and icebergs from the

801 Arctic Ocean (Not and Hillaire-Marcel, 2012) may have triggered the YD cooling
802 event and the decline of AMOC strength (Tarasov and Peltier, 2005; Condron and
803 Winsor, 2012), which occurred at about 12.7 ka (McManus et al., 2004; see Fig. 10h).
804 In this hypothesis, the opening of the Bering Strait could well have led to enhanced
805 southward export of sea ice through Fram Strait and to the weakening of the AMOC
806 as simulated by Hu et al. (2015) from Community Climate System Model
807 experiments.

808

809 6.3 The setting of full ‘‘interglacial’’ conditions

810

811 The Holocene has been climatically more stable than the deglaciation. However,
812 many studies point to significant variations of sea-surface conditions on a regional
813 scale, especially during the early Holocene which was marked by delayed
814 establishment of optimal temperature in response to the high-latitude insolation
815 maximum at 10 ka (e.g., Solignac et al., 2004; de Vernal and Hillaire-Marcel, 2006;
816 Bonnet et al., 2010; Werner et al., 2011, 2013, 2016; de Vernal et al., 2013; Van
817 Nieuwenhove et al., 2016; Zumaque et al., 2017).

818

819 In the eastern Fram Strait, our results show that the transition towards modern-like
820 conditions occurred in surface water from the end of the YD to about 7.6 ka. It was
821 marked by an increase in SSSs, likely in relation to the diminution of meltwater
822 discharges after continental glaciers finally resumed. This transition was also
823 characterized by decreasing stratification of the upper water mass, accompanied by a
824 decreased gradient of seasonal SSTs. The recovery of the AMOC after 11.7 ka,
825 lasting until about 8 ka, was also suggested from ^{231}Pa data (cf. McManus, 2004; see
826 Fig. 10h). Intensification of the Transpolar Drift (Not and Hillaire-Marcel, 2012)
827 together with enhanced penetration of AW into the Arctic Ocean might also have

828 intensified turbulence in the water column, thus contributing to changes in the
829 stratification in the Fram Strait.

830

831 In our records, there is a tenuous SST optimum in summer from 10.5 to 8.5 ka. It is
832 characterized by low, but significant occurrences of the temperate taxa *Spiniferites*
833 *mirabilis* at site MSM5-712 and *Impagidinium sphaericum* at site PS2863 (Fig. 4),
834 which lead to reconstruct mean summer SSTs of about 2.5°C higher than those of the
835 late Holocene at site MSM5-712 (Fig. 6a) and minimum sea-ice cover extent at site
836 PS2863 (Fig. 8d). In core MSM5-712, high amplitude variations in summer SSTs and
837 salinity suggest unstable conditions possibly due to episodic freshwater supply
838 accompanied with oscillation of the Arctic Coastal Front.

839

840 In subsurface waters, foraminifer data indicate that temperatures started to increase
841 by about 11 ka, highlighting enhanced northward heat fluxes through the AW with
842 maximum values reached at about 10 ka (Hald et al., 2007; Risebrobakken et al.,
843 2011; Werner et al., 2016). However, the alkenone-based surface temperatures
844 reached their maximum values later, between 9 and 6 ka south of Svalbard (Calvo et
845 al., 2002; Marchal et al., 2002). The postglacial sea-surface warming generally
846 occurred later, at about 8.5 ka in the southeastern Norwegian Sea and at various
847 locations of the northern North Atlantic, according to diatom data (Koç and Jansen,
848 1992; Andersen et al., 2004a). The differences in timing of the establishment of the
849 temperature optimum might, at least in part, be due to seasonal biases depending
850 upon the proxy used (e.g., Sejrup et al., 2016). Nevertheless, all proxies tend to
851 indicate that the early Holocene was marked by regionalism in the changes of ocean
852 conditions.

853

854 The beginning of Zone I is marked by increased dinocyst concentrations at both sites,
855 reaching maximum values at the top of the cores (Fig. 3 a, f). The concentrations are,
856 however, lower at site PS2863, possibly because of lower productivity due to lower
857 nutrient inputs. An important transition in dinocyst assemblages occurred at ca. 7.6 ka
858 when *O. centrocarpum* became dominant and the relative abundances of the main
859 taxa reached values close to modern ones, thus leading to define Zone I (Fig. 4). The
860 shift in dinocyst assemblages at about 8-7.5 ka, which corresponds to an abrupt
861 decrease in *N. labyrinthus* at the benefit of *O. centrocarpum*, has been noticed in
862 many other cores from the southern Norwegian Sea and the Fram Strait (Baumann
863 and Matthiessen, 1992; Matthiessen and Baumann, 1997; Van Nieuwenhove et al.,
864 2016). This change in Nordic Seas was dated slightly later, at 7.5-6 ka, and has been
865 interpreted as being related to a major reorganization in ocean circulation (Van
866 Nieuwenhove et al., 2016). Furthermore, the maximum $\delta^{13}\text{C}$ values in both planktic
867 and benthic foraminifers from the deep Greenland Sea point to a setting with
868 maximum deep-water renewal at about the same time (Bauch et al., 2001; Telesinski
869 et al., 2014). Similarly, a transition at 7.5-6 ka, near the beginning of Zone I, is
870 recorded in coccolith assemblages of the Nordic Seas, which also suggests an
871 important change in the sea-surface conditions and the establishment of modern
872 ocean properties (Matthiessen et al., 1992). Finally, it is of note that *Pediastrum* is
873 nearly absent in Zone I, which suggests limited input of freshwater.

874

875 The dinocysts of the Mid to Late Holocene interval show low amplitude variations. A
876 cooling trend was depicted as illustrated by a decrease in winter SSTs of about 1.5°C
877 and an increase in sea-ice cover of 1-2 months/yr at both study sites (Fig. 9a, c). The
878 SST decrease is coherent with the subsurface cooling recorded after 7.9 ka and 5 ka
879 from planktic foraminifer data (Werner et al., 2013, 2016; Aagaard-Sørensen et al.,
880 2014a). It corresponds to the establishment of the modern sea-ice factory on the East

881 Siberian Arctic shelves (cf. Werner et al., 2013, 2016). A minor warming was
882 however recorded during the last 3000 years in subsurface waters from Mg/Ca data
883 (Aagaard-Sørensen et al., 2014a) and transfer functions applied to planktic
884 foraminifer assemblages (Werner et al., 2013, 2016). Such warming could be due to
885 limited heat loss at the surface due to stratification fostered by fresh surface waters
886 originating from the melt of sea ice and/or icebergs. Decoupling between surface and
887 subsurface waters would thus result from sea-ice cover increase that forced planktic
888 foraminifers to dwell deeper in the water column into warmer waters more insulated
889 subsurface AW in the Nordic Seas.

890

891 **7. Conclusions**

892

893 The dinocyst assemblages document important shifts in sea-surface conditions over
894 the last 23,000 years at two sites in the northeastern Fram Strait. The ecological
895 preferences of the taxa and the application of a quantitative modern analog technique
896 permit to document seasonal SSTs, SSSs and sea-ice cover. Hence, our records
897 provide insights into the relationship between meltwater inputs and AW inflows
898 throughout the deglaciation, as the approach permits to disentangle salinity and
899 temperature signals as well as the SSTs from winter and summer. Our records also
900 reveal changes in the sea-surface circulation of northeastern Fram Strait during the
901 deglaciation and the early Holocene.

902

903 The LGM was characterized by special hydrographic conditions in the Nordic Seas
904 and the paleoceanographic reconstructions to date remain equivocal as they illustrate
905 cold to relatively warm conditions depending upon the proxies used (cf. de Vernal et
906 al., 2006) During the LGM, there was probably some AW heat advection. However,
907 low dinocyst fluxes lead us to hypothesize that the inflows of AW to the surface

908 might have been episodic, causing short-lived events of open waters throughout an
909 interval otherwise characterized by generally harsh conditions. A sedimentary record
910 of higher temporal resolution would allow to test such hypothesis.

911

912 The deglaciation started between 19 and 18 ka in the northeastern Fram Strait which
913 remained under the influence of major meltwater discharges resulting in low salinity
914 until about 12.6 ka. During the deglaciation, a warm episode, likely related to strong
915 AW inflows, was recorded between 14.7 and 12.6 ka. It was interrupted by a cooling
916 event dated of 14.5-14.1 ka at site MSM5-712 and probably related to the enhanced
917 calving of the Barents Sea ice sheet, which can be associated with the rapid
918 deposition of a ubiquitous fine grain sediment layer along the northwestern Barents
919 Sea and western Svalbard continental slopes (Jessen et al., 2010; Lucchi et al., 2015).
920 The ice surge and subsequent cooling could have been triggered by the influence of
921 warm AW inflows. Hence, during the deglaciation the advection of heat would have
922 led to enhanced melting of the SBSIS.

923

924 During the YD, particularly from 12.6 to 12 ka, there was a major change towards
925 colder but more saline conditions, suggesting reduced meltwater inputs. The YD was
926 also a transition marked by the onset of coastal fronts at the western and northern
927 margins of Svalbard as the result of enhanced contribution of Arctic waters. The
928 transition towards full interglacial conditions was marked by increasing salinity until
929 modern like values were reached at about 7.6 ka. During the Mid to Late Holocene, a
930 general cooling trend was detected mostly from a decrease in winter SSTs.

931

932 Our study combining SST and SSS reconstructions permitted to identify important
933 climate-related parameters like meltwater discharges and stratification of the surface
934 water layer. The major transitions in sea-surface conditions, notably those which

935 occurred shortly after the onset of the BA and the YD, seem closely related to shifts
936 in the AMOC strength as reconstructed from mid latitude North Atlantic geochemical
937 data (e.g., McManus et al., 2004) (Fig. 10). This relation points to high sensitivity of
938 eastern Fram Strait to AW inflow intensity and its critical role in ocean circulation.

939

940 **8. Acknowledgements**

941

942 This study was supported by the *Fonds Québécois de la Recherche sur la Nature et*
943 *les Technologies* (FQRNT), the Natural Sciences and Engineering Research Council
944 of Canada (NSERC), and the Academy of Sciences, Humanities and Literature Mainz
945 through the *Akademienprogramm*. The laboratory analyses have been possible thanks
946 to the GEOTOP facilities. The sediment samples from cores PS2863-1 and PS2832-
947 2BC were made available through the ARK-XIII/2 expedition of the *RV Polarstern*
948 and through the MSM05/5b expedition of the *RV Maria S. Merian* for core MSM5/5-
949 712-2. A ^{14}C age was operated by the NOSAMS facility at the Woods Hole
950 Oceanographic Institution with National Science Foundation sponsorship (OCE-
951 1239667). Special thanks go to Maryse Henry and Sophie Bonnet for the
952 palynological analysis of the first 315 cm of the MSM5/5-712-2 core. We thank
953 Simon Van Bellen for his help in developing the age models from the Bacon
954 software. We are grateful to the three anonymous reviewers of the journal for their
955 critical comments on the original manuscript.

956

957 **9. References**

958

959 Aagaard-Sørensen, S., Husum, K., Hald, M., Marchitto, T., Godtlielsen, F., 2014a.
960 Sub sea surface temperatures in the Polar North Atlantic during the

- 961 Holocene: Planktic foraminiferal Mg/Ca temperature reconstructions. *The*
962 *Holocene* 24, 93-103.
- 963 Aagaard-Sørensen, S., Husum, K., Werner, K., Spielhagen, R.F., Hald, M.,
964 Marchitto, T.M., 2014b. A Late Glacial–Early Holocene multiproxy record
965 from the eastern Fram Strait, Polar North Atlantic. *Marine Geology* 355, 15-
966 26.
- 967 Allan, E., de Vernal, A., Knudsen, Hillaire-Marcel, C., Moros, M., Ribeiro, S.,
968 Ouellet-Bernier, M.-M., Seidenkrantz, M.-S., 2018. Sea-surface instabilities
969 in the Disko Bugt area, west Greenland, in phase with $\delta^{18}\text{O}$ -oscillations at
970 Camp Century reveals climatic change during the late Holocene.
971 *Paleoceanography and Paleoclimatology*, 33.
- 972 Alley, R.B., 2000. The Younger Dryas cold interval as viewed from central
973 Greenland. *Quaternary science reviews* 19, 213-226.
- 974 Andersen, E.S., Dokken, T.M., Elverhøi, A., Solheim, A., Fossen, I., 1996. Late
975 Quaternary sedimentation and glacial history of the western Svalbard
976 continental margin. *Marine Geology* 133, 123-156.
- 977 Andersen, C., Koç, N., Moros, M., 2004a. A highly unstable Holocene climate in the
978 subpolar North Atlantic: evidence from diatoms. *Quaternary Science*
979 *Reviews* 23, 2155-2166.
- 980 Andersen, K.K., Azuma, N., Barnola, J.-M., Bigler, M., Biscaye, P., Caillon, N.,
981 Chappellaz, J., Clausen, H.B., Dahl-Jensen, D., Fischer, H., 2004b. High-
982 resolution record of Northern Hemisphere climate extending into the last
983 interglacial period. *Nature* 431, 147-151.
- 984 Bartels, M., Titschack, J., Fahl, K., Stein, R., Seidenkrantz, M.-S., Hillaire-Marcel,
985 C., Hebbeln, D., 2017. Atlantic Water advection vs. glacier dynamics in
986 northern Spitsbergen since early deglaciation. *Climate of the Past* 13, 1717.

- 987 Bauch, H.A., Erlenkeuser, H., Spielhagen, R.F., Struck, U., Matthiessen, J., Thiede,
988 J., Heinemeier, J., 2001. A multiproxy reconstruction of the evolution of deep
989 and surface waters in the subarctic Nordic seas over the last 30,000 yr.
990 *Quaternary Science Reviews* 20, 659-678.
- 991 Baumann, K.-H., Matthiessen, J., 1992. Variations in surface water mass conditions
992 in the Norwegian Sea: evidence from Holocene coccolith and dinoflagellate
993 cyst assemblages. *Marine Micropaleontology* 20, 129-146.
- 994 Blaauw, M., Christen, J.A., 2011. Flexible paleoclimate age-depth models using an
995 autoregressive gamma process. *Bayesian Analysis* 6, 457-474.
- 996 Bond, G., Broecker, W., Johnsen, S., McManus, J., Labeyrie, L., Jouzel, J., Bonani,
997 G., 1993. Correlations between climate records from North Atlantic
998 sediments and Greenland ice. *Nature* 365, 143-147.
- 999 Bonnet, S., de Vernal, A., Hillaire-Marcel, C., Radi, T., Husum, K., 2010. Variability
1000 of sea-surface temperature and sea-ice cover in the Fram Strait over the last
1001 two millennia. *Marine Micropaleontology* 74, 59-74.
- 1002 Budéus, G., 2007. Short Cruise Report RV Maria S. Merian Cruise MSM05/5.
1003 University of Hamburg, Institute of Oceanography.
- 1004 Calvo, E., Grimalt, J., Jansen, E., 2002. High resolution U 37 K sea surface
1005 temperature reconstruction in the Norwegian Sea during the Holocene.
1006 *Quaternary Science Reviews* 21, 1385-1394.
- 1007 Chauhan, T., Rasmussen, T., Noormets, R., Jakobsson, M., Hogan, K., 2014. Glacial
1008 history and paleoceanography of the southern Yermak Plateau since 132 ka
1009 BP. *Quaternary Science Reviews* 92, 155-169.
- 1010 Chauhan, T., Rasmussen, T.L., Noormets, R., 2016. Palaeoceanography of the
1011 Barents Sea continental margin, north of Nordaustlandet, Svalbard, during
1012 the last 74 ka. *Boreas* 45, 76-99.

- 1013 Condron, A., Winsor, P., 2012. Meltwater routing and the Younger Dryas.
1014 Proceedings of the National Academy of Sciences 109, 19928-19933.
- 1015 Conkright, M.E., Locarnini, R.A., Garcia, H.E., O'Brien, T.D., Boyer, T.P., Stephens,
1016 C., Antonov, J.I., 2002. World Ocean Atlas 2001: Objective analyses, data
1017 statistics, and figures: CD-ROM documentation. US Department of
1018 Commerce, National Oceanic and Atmospheric Administration, National
1019 Oceanographic Data Center, Ocean Climate Laboratory.
- 1020 Consolaro, C., Rasmussen, T.L., Panieri, G., 2018. Palaeoceanographic and
1021 environmental changes in the eastern Fram Strait during the last 14,000 years
1022 based on benthic and planktonic foraminifera. *Marine Micropaleontology*
1023 139, 84–101.
- 1024 Cronin, T.M., Dwyer, G.S., Farmer, J., Bauch, H.A., Spielhagen, R.F., Jakobsson,
1025 M., Nilsson, J., Briggs Jr, W., Stepanova, A., 2012. Deep Arctic Ocean
1026 warming during the last glacial cycle. *Nature Geoscience* 5, 631-634.
- 1027 de Vernal, A., Bilodeau, G., Hillaire-Marcel, C., Kassou, N., 1992. Quantitative
1028 assessment of carbonate dissolution in marine sediments from foraminifer
1029 linings vs. shell ratios: Davis Strait, northwest North Atlantic. *Geology* 20,
1030 527-530.
- 1031 de Vernal, A., Hillaire-Marcel, C., Turon, J., Matthiessen, J., Rochon, A., Vallières,
1032 S., Levesque, L., 2000. Sea-surface conditions in middle to high latitudes of
1033 the North Atlantic during the last glacial maximum (LGM): the cold
1034 paradigm revisited. *Canadian Journal of Earth Sciences* 37, 725-750.
- 1035 de Vernal, A., Henry, M., Matthiessen, J., Mudie, P.J., Rochon, A., Boessenkool,
1036 K.P., Eynaud, F., Grøsfjeld, K., Guiot, J., Hamel, D., Harland, R., Head,
1037 M.J., Kunz-Pirrung, M., Levac, E., Loucheur, V., Peyron, O., Pospelova, V.,
1038 Radi, T., Turon, J.-L., Voronina, E., 2001. Dinoflagellate cyst assemblages as
1039 tracers of sea-surface conditions in the northern North Atlantic, Arctic and

- 1040 sub-Arctic seas: the new 'n= 677' data base and its application for
1041 quantitative palaeoceanographic reconstruction. *Journal of Quaternary*
1042 *Science* 16, 681-698.
- 1043 de Vernal, A., Eynaud, F., Henry, M., Hillaire-Marcel, C., Londeix, L., Mangin, S.,
1044 Matthiessen, J., Marret, F., Radi, T., Rochon, A., Solignac, S., Turon, J.L.,
1045 2005. Reconstruction of sea-surface conditions at middle to high latitudes of
1046 the Northern Hemisphere during the Last Glacial Maximum (LGM) based on
1047 dinoflagellate cyst assemblages. *Quaternary Science Reviews* 24, 897-924.
- 1048 de Vernal, A., Hillaire-Marcel, C., 2006. Provincialism in trends and high frequency
1049 changes in the northwest North Atlantic during the Holocene. *Global and*
1050 *Planetary Change* 54, 263-290.
- 1051 de Vernal, A., Rosell-Melé, A., Kucera, M., Hillaire-Marcel, C., Eynaud, F., Weinelt,
1052 M., Dokken, T., Kageyama, M., 2006. Comparing proxies for the
1053 reconstruction of LGM sea-surface conditions in the northern North Atlantic.
1054 *Quaternary Science Reviews* 25, 2820-2834.
- 1055 de Vernal, A., Bilodeau, G., Henry, M., 2010. Micropaleontological preparation
1056 techniques and analyses. *Cahier du Geotop*.
- 1057 de Vernal, A., Hillaire-Marcel, C., Rochon, A., Fréchette, B., Henry, M., Solignac, S.,
1058 Bonnet, S., 2013. Dinocyst-based reconstructions of sea ice cover
1059 concentration during the Holocene in the Arctic Ocean, the northern North
1060 Atlantic Ocean and its adjacent seas. *Quaternary Science Reviews* 79, 111-
1061 121.
- 1062 Dodge, J., 1989. Some revisions of the family Gonyaulacaceae (Dinophyceae) based
1063 on a scanning electron microscope study. *Botanica marina* 32, 275-298.
- 1064 Dokken, T.M., Jansen, E., 1999. Rapid changes in the mechanism of ocean
1065 convection during the last glacial period. *Nature* 401, 458-461.

- 1066 Ellegaard, M., 2000. Variations in dinoflagellate cyst morphology under conditions of
1067 changing salinity during the last 2000 years in the Limfjord, Denmark.
1068 *Review of Palaeobotany and Palynology* 109, 65-81.
- 1069 Eynaud, F., Duprat, J., Turon, J.-L., Zaragosi, S., 2004. Paleohydrological evidence
1070 of a two step evolution of the Last Glacial Maximum (LGM) along the
1071 western European margins. Eighth International Conference on
1072 Paleooceanography, Biarritz, September, Programme and abstracts, B1-153.
- 1073 Fahrbach, E., Meincke, J., Østerhus, S., Rohardt, G., Schauer, U., Tverberg, V.,
1074 Verduin, J., 2001. Direct measurements of volume transports through Fram
1075 Strait. *Polar Research* 20, 217-224.
- 1076 Falardeau, J., 2017. Paléocéanographie du nord-est du Déroit de Fram depuis le
1077 dernier maximum glaciaire. Université du Québec à Montréal.
- 1078 Fetterer, F., Knowles, K., Meier, W., Savoie, M., 2016. Sea Ice Index, Version 2.
1079 National Snow and Ice Data Center, Boulder, CO, USA. Digital Media,
1080 updated daily.
- 1081 Forwick, M., Vorren, T.O., 2009. Late Weichselian and Holocene sedimentary
1082 environments and ice rafting in Isfjorden, Spitsbergen. *Palaeogeography,*
1083 *Palaeoclimatology, Palaeoecology* 280, 258-274.
- 1084 Gascard, J.-C., Richez, C., Rouault, C., 1995. New insights on large-scale
1085 oceanography in Fram Strait: The West Spitsbergen Current. 49, 131-182.
- 1086 Gibb, O.T., Hillaire-Marcel, C., de Vernal, A., 2014. Oceanographic regimes in the
1087 northwest Labrador Sea since Marine Isotope Stage 3 based on dinocyst and
1088 stable isotope proxy records. *Quaternary Science Reviews* 92, 269-279.
- 1089 Giraudeau, J., (in preparation). EPOC (University Bordeaux 1/CNRS) within the
1090 framework of an ongoing IFM-GEOMAR. EPOC collaboration.

- 1091 Grøsfjeld, K., Harland, R., Howe, J., 2009. Dinoflagellate cyst assemblages inshore
1092 and offshore Svalbard reflecting their modern hydrography and climate.
1093 Norwegian Journal of Geology 89, 121-134.
- 1094 Guiot, J., 1990. Methodology of the last climatic cycle reconstruction in France from
1095 pollen data. *Palaeogeography, Palaeoclimatology, Palaeoecology* 80, 49-69.
- 1096 Guiot, J., de Vernal, A., 2007. Transfer functions: methods for quantitative
1097 paleoceanography based on microfossils. In: Hillaire-Marcel, C., de Vernal,
1098 A. (Eds.) *Proxies in Late Cenozoic Paleoceanography*. Elsevier, pp. 523-563.
- 1099 Guiot, J., de Vernal, A., 2011. Is spatial autocorrelation introducing biases in the
1100 apparent accuracy of paleoclimatic reconstructions? *Quaternary Science*
1101 *Reviews* 30: 1965-1972.
- 1102 Hald, M., Dokken, T., Mikalsen, G., 2001. Abrupt climatic change during the last
1103 interglacial–glacial cycle in the polar North Atlantic. *Marine Geology* 176,
1104 121-137.
- 1105 Hald, M., Andersson, C., Ebbesen, H., Jansen, E., Klitgaard-Kristensen, D.,
1106 Risebrobakken, B., Salomonsen, G.R., Sarnthein, M., Sejrup, H.P., Telford,
1107 R.J., 2007. Variations in temperature and extent of Atlantic Water in the
1108 northern North Atlantic during the Holocene. *Quaternary Science Reviews*
1109 26, 3423-3440.
- 1110 Hall, I.R., Moran, S., Zahn, R., Knutz, P.C., Shen, C.C., Edwards, R., 2006.
1111 Accelerated drawdown of meridional overturning in the late- glacial Atlantic
1112 triggered by transient pre- H event freshwater perturbation. *Geophysical*
1113 *Research Letters* 33.
- 1114 Hamel, D., de Vernal, A., Gosselin, M., Hillaire-Marcel, C., 2002. Organic-walled
1115 microfossils and geochemical tracers: sedimentary indicators of productivity
1116 changes in the North Water and northern Baffin Bay during the last centuries.
1117 *Deep Sea Research Part II: Topical Studies in Oceanography* 49, 5277-5295.

- 1118 Hebbeln, D., Dokken, T., Andersen, E.S., Hald, M., Elverhøi, A., 1994. Moisture
1119 supply for northern ice-sheet growth during the Last Glacial Maximum.
- 1120 Hebbeln, D., Wefer, G., 1997. Late Quaternary paleoceanography in the Fram Strait.
1121 *Paleoceanography* 12, 65-78.
- 1122 Heinrich, H., 1988. Origin and consequences of cyclic ice rafting in the Northeast
1123 Atlantic Ocean during the past 130,000 years. *Quaternary Research* 29, 142-
1124 152.
- 1125 Hemming, S. R., 2004. Heinrich events: Massive late Pleistocene detritus layers of
1126 the North Atlantic and their global climate imprint. *Reviews of Geophysics*
1127 42: RG1005
- 1128 Hillaire-Marcel, C., Maccali, J., Not, C., Poirier, A., 2013. Geochemical and isotopic
1129 tracers of Arctic sea ice sources and export with special attention to the
1130 Younger Dryas interval. *Quaternary Science Reviews* 79, 184-190.
- 1131 Hu, A., Meehl, G.A., Han, W., Otto-Blietner, B., Abe-Ouchi, A., Rosenbloom, N.,
1132 2015. Effects of the Bering Strait closure on AMOC and global climate under
1133 different background climates. *Progress in Oceanography* 132, 174-196.
- 1134 Hughes, A.L., Gyllencreutz, R., Lohne, Ø.S., Mangerud, J., Svendsen, J.I., 2016. The
1135 last Eurasian ice sheets—a chronological database and time- slice
1136 reconstruction, DATED- 1. *Boreas* 45, 1-45.
- 1137 Ivanovic, R., Grégoire, L., Wickert, A., Burke, A., Valdes, P., 2017. Heinrich Stadial
1138 1 caused by acceleration of Eurasian deglaciation ~18.5 ka, Abstract
1139 *Goldschmidt 2017*.
- 1140 Jessen, S.P., Rasmussen, T.L., Nielsen, T., Solheim, A., 2010. A new Late
1141 Weichselian and Holocene marine chronology for the western Svalbard slope
1142 30,000–0 cal years BP. *Quaternary Science Reviews* 29, 1301-1312.
- 1143 Jones, G.A., Keigwin, L.D., 1988. Evidence from Fram Strait (78 N) for early
1144 deglaciation. *Nature* 336, 56-59.

- 1145 Jorissen, F.J., Fontanier, C., Thomas, E., 2007. Chapter seven paleoceanographical
1146 proxies based on deep-sea benthic foraminiferal assemblage characteristics.
1147 *Developments in Marine Geology* 1, 263-325.
- 1148 Koç, N., Jansen, E., 1992. A high- resolution diatom record of the last deglaciation
1149 from the SE Norwegian Sea: Documentation of rapid climatic changes.
1150 *Paleoceanography* 7, 499-520.
- 1151 Koç, N., Klitgaard-Kristensen, D., Hasle, K., Forsberg, C.F., Solheim, A., 2002. Late
1152 glacial palaeoceanography of Hinlopen Strait, northern Svalbard. *Polar*
1153 *Research* 21, 307-314.
- 1154 Kodrans-Nsiah, M., de Lange, G.J., Zonneveld, K.A.F., 2008. A natural exposure
1155 experiment on short-term species-selective aerobic degradation of
1156 dinoflagellate cysts. *Review of Palaeobotany and Palynology* 152, 32-39.
- 1157 Kucera, M., Rosell-Melé, A., Schneider, R., Waelbroeck, C., Weinelt, M., 2005.
1158 Multiproxy approach for the reconstruction of the glacial ocean surface
1159 (MARGO). *Quaternary Science Reviews* 24, 813-819.
- 1160 Kristensen, D.K., Rasmussen, T.L., Koç, N., 2013. Palaeoceanographic changes in
1161 the northern Barents Sea during the last 16 000 years—new constraints on the
1162 last deglaciation of the Svalbard–Barents Sea Ice Sheet. *Boreas* 42, 798-813.
- 1163 Landvik, J.Y., Mangerud, J., Salvigsen, O., 1987. The Late Weichselian and
1164 Holocene shoreline displacement on the west- central coast of Svalbard.
1165 *Polar Research* 5, 29-44.
- 1166 Landvik, J.Y., Bondevik, S., Elverhøi, A., Fjeldskaar, W., Mangerud, J., Salvigsen,
1167 O., Siegert, M.J., Svendsen, J.-I., Vorren, T.O., 1998. The last glacial
1168 maximum of Svalbard and the Barents Sea area: ice sheet extent and
1169 configuration. *Quaternary Science Reviews* 17, 43-75

- 1170 Laskar, J., Robutel, P., Joutel, F., Gastineau, M., Correia, A., Levrard, B., 2004. A
1171 long-term numerical solution for the insolation quantities of the Earth.
1172 *Astronomy & Astrophysics* 428, 261-285.
- 1173 Leduc, J., 2001. Study of benthic foraminiferal populations in the sediments of the
1174 Saguenay fjord. Université du Québec à Montréal.
- 1175 Lehman, S., Jones, G., Keigwin, L., Andersen, E., Butenkoi, G., Østmo, S., 1991.
1176 Initiation of Fennoscandian ice-sheet retreat during the last deglaciation.
- 1177 Levine, R.C., Bigg, G.R., 2008. Sensitivity of the glacial ocean to Heinrich events
1178 from different iceberg sources, as modeled by a coupled atmosphere-
1179 iceberg- ocean model. *Paleoceanography* 23.
- 1180 Loeng, H., 1991. Features of the physical oceanographic conditions of the Barents
1181 Sea. *Polar research* 10, 5-18.
- 1182 Lucchi, R.G., Sagnotti, L., Camerlenghi, A., Macrì, P., Rebesco, M., Pedrosa, M.T.,
1183 Giorgetti, G., 2015. Marine sedimentary record of Meltwater Pulse 1a along
1184 the NW Barents Sea continental margin. *arktos* 1, 7.
- 1185 Mangerud, J., 1972. Radiocarbon dating of marine shells, including a discussion of
1186 apparent age of recent shells from Norway. *Boreas* 1, 143-172.
- 1187 Mangerud, J., Gulliksen, S., 1975. Apparent radiocarbon ages of recent marine shells
1188 from Norway, Spitsbergen, and Arctic Canada. *Quaternary Research* 5, 263-
1189 273.
- 1190 Mangerud, J., Landvik, J.Y., 2007. Younger Dryas cirque glaciers in western
1191 Spitsbergen: smaller than during the Little Ice Age. *Boreas* 36, 278-285.
- 1192 Manley, T., 1995. Branching of Atlantic Water within the Greenland- Spitsbergen
1193 Passage: An estimate of recirculation. *Journal of Geophysical Research:*
1194 *Oceans* 100, 20627-20634.
- 1195 Marchal, O., Cacho, I., Stocker, T.F., Grimalt, J.O., Calvo, E., Martrat, B.,
1196 Shackleton, N., Vautravers, M., Cortijo, E. et van Kreveld, S., 2002.

- 1197 Apparent long-term cooling of the sea surface in the northeast Atlantic and
1198 Mediterranean during the Holocene. *Quaternary Science Reviews*, 21(4),
1199 455-483.
- 1200 Marret, F., Zonneveld, K.A., 2003. Atlas of modern organic-walled dinoflagellate
1201 cyst distribution. *Review of Palaeobotany and Palynology* 125, 1-200.
- 1202 Maslowski, W., Marble, D., Walczowski, W., Schauer, U., Clement, J.L., Semtner,
1203 A.J., 2004. On climatological mass, heat, and salt transports through the
1204 Barents Sea and Fram Strait from a pan-Arctic coupled ice-ocean model
1205 simulation. *Journal of Geophysical Research: Oceans* 109.
- 1206 Matthews, J., 1969. The assessment of a method for the determination of absolute
1207 pollen frequencies. *New Phytologist* 68, 161-166.
- 1208 Matthiessen, J., 1995. Distribution patterns of dinoflagellate cysts and other organic-
1209 walled microfossils in recent Norwegian-Greenland Sea sediments. *Marine*
1210 *Micropaleontology* 24, 307-334.
- 1211 Matthiessen, J., Baumann, A., 1997. Dinoflagellate cyst records from the East
1212 Greenland continental margin during the last 15,000 years: implications for
1213 paleoceanographic reconstructions, in: Hass, H.C. & Kaminski, M.A. (Eds.),
1214 *Contributions to the Micropaleontology and Paleoceanography of the*
1215 *Northern North Atlantic*. Gryzbowski Foundation Special Publication, pp.
1216 149-165.
- 1217 McManus, J.F., Francois, R., Gherardi, J.-M., Keigwin, L.D., Brown-Leger, S., 2004.
1218 Collapse and rapid resumption of Atlantic meridional circulation linked to
1219 deglacial climate changes. *Nature* 428, 834-837.
- 1220 Mertens, K.N., Bringué, M., Van Nieuwenhove, N., Takano, Y., Pospelova, V.,
1221 Rochon, A., De Vernal, A., Radi, T., Dale, B., Patterson, R.T., Weckström,
1222 K., Andrén, E., Louwey, S., Matsuoka, K., 2012. Process length variation of
1223 the cyst of the dinoflagellate *Protoceratium reticulatum* in the North Pacific

- 1224 and Baltic-Skagerrak region: calibration as an annual density proxy and first
1225 evidence of pseudo-cryptic speciation. *Journal of Quaternary Science* 27,
1226 734-744.
- 1227 Müller, J., Werner, K., Stein, R., Fahl, K., Moros, M., Jansen, E., 2012. Holocene
1228 cooling culminates in sea ice oscillations in Fram Strait. *Quaternary Science*
1229 *Reviews* 47, 1-14.
- 1230 Müller, J., Stein, R., 2014. High-resolution record of late glacial and deglacial sea ice
1231 changes in Fram Strait corroborates ice–ocean interactions during abrupt
1232 climate shifts. *Earth and Planetary Science Letters* 403, 446-455.
- 1233 National Snow and Ice Data Center (NSIDC), 2003. Brightness temperature and ice
1234 concentrations grids for the polar regions. Boulder, CO: NSIDC Distributed
1235 Active Archive Center.
- 1236 Nørgaard-Pedersen, N., Spielhagen, R.F., Erlenkeuser, H., Grootes, P.M.,
1237 Heinemeier, J., Knies, J., 2003. Arctic Ocean during the Last Glacial
1238 Maximum: Atlantic and polar domains of surface water mass distribution and
1239 ice cover. *Paleoceanography* 18 (3), 1063.
- 1240 Not, C., Hillaire-Marcel, C., 2012. Enhanced sea-ice export from the Arctic during
1241 the Younger Dryas. *Nature Communications* 3, 647.
- 1242 Olsson, I.U., 1980. Content of ^{14}C in marine mammals from northern Europe.
1243 *Radiocarbon* 22, 662-675.
- 1244 Pflaumann, U., Sarnthein, M., Chapman, M., d'Abreu, L., Funnell, B., Huels, M.,
1245 Kiefer, T., Maslin, M., Schulz, H., Swallow, J., van Kreveld, S., Vautravers,
1246 M., Vogelsang, E., Weinelt, M., 2003. Glacial North Atlantic: Sea-surface
1247 conditions reconstructed by GLAMAP 2000. *Paleoceanography* 18 (3), 1065.
- 1248 Rasmussen, S.O., Andersen, K.K., Svensson, A.M., Steffensen, J.P., Vinther, B.M.,
1249 Clausen, H.B., Siggaard-Andersen, M.L., Johnsen, S.J., Larsen, L.B., Dahl-
1250 Jensen, D., Bigler, M., Röthlisberger, R., Fischer, H., Goto-Azuma, K.,

- 1251 Hansson, M.E., Ruth, U., 2006. A new Greenland ice core chronology for the
1252 last glacial termination. *Journal of Geophysical Research* 111.
- 1253 Rasmussen, T.L., Thomsen, E., Ślubowska, M.A., Jessen, S., Solheim, A., Koç, N.,
1254 2007. Paleoceanographic evolution of the SW Svalbard margin (76°N) since
1255 20,000 14C yr BP. *Quaternary Research* 67, 100-114.
- 1256 Rasmussen, T.L., Thomsen, E., 2008. Warm Atlantic surface water inflow to the
1257 Nordic seas 34–10 calibrated ka BP. *Paleoceanography* 23.
- 1258 Rasmussen, T.L., Forwick, M., Mackensen, A., 2012. Reconstruction of inflow of
1259 Atlantic Water to Isfjorden, Svalbard during the Holocene: Correlation to
1260 climate and seasonality. *Marine Micropaleontology* 94-95, 80-90.
- 1261 Rasmussen, T., Thomsen, E., 2014. Brine formation in relation to climate changes
1262 and ice retreat during the last 15,000 years in Storfjorden, Svalbard, 76–
1263 78°N. *Paleoceanography* 29, 911-929.
- 1264 Reimer, P.J., Bard, E., Bayliss, A., Beck, J.W., Blackwell, P.G., Bronk Ramsey, C.,
1265 Buck, C.E., Cheng, H., Edwards, R.L., Friedrich, M., 2013. IntCal13 and
1266 Marine13 radiocarbon age calibration curves 0-50,000 years cal BP.
- 1267 Reusche, M., Winsor, K., Carlson, A.E., Marcott, S.A., Rood, D.H., Novak, A., Roof,
1268 S., Retelle, M., Werner, A., Caffee, M., 2014. 10 Be surface exposure ages on
1269 the late-Pleistocene and Holocene history of Linnébreen on Svalbard.
1270 *Quaternary Science Reviews* 89, 5-12.
- 1271 Risebrobakken, B., Dokken, T., Smedsrud, L.H., Andersson, C., Jansen, E., Moros,
1272 M., Ivanova, E.V., 2011. Early Holocene temperature variability in the
1273 Nordic Seas: The role of oceanic heat advection versus changes in orbital
1274 forcing. *Paleoceanography* 26.
- 1275 Rochon, A., Vernal, A.d., Turon, J.-L., Matthiessen, J., Head, M., 1999. Distribution
1276 of recent dinoflagellate cysts in surface sediments from the North Atlantic

- 1277 Ocean and adjacent seas in relation to sea-surface parameters. American
1278 Association of Stratigraphic Palynologists Contribution Series 35, 1-146.
- 1279 Rochon, A., Mudie, P.J., Aksu, A.E., Gillespie, H., 2002. Pterocystagen. nov.: A new
1280 dinoflagellate cyst from pleistocene glacial- stage sediments of the black and
1281 Marmara Seas. *Palynology* 26, 95-105.
- 1282 Rochon, A., Lewis, J., Ellegaard, M., Harding, I.C., 2009. The *Gonyaulax spinifera*
1283 (Dinophyceae) “complex”: Perpetuating the paradox? Review of
1284 *Palaeobotany and Palynology* 155, 52-60.
- 1285 Rørvik, K.L., Rasmussen, T.L., Hald, M., Husum, K., 2013. Intermediate water
1286 ventilation in the Nordic seas during MIS 2. *Geophysical Research Letters* 40,
1287 1805-1810.
- 1288 Rosell-Melé, A., Comes, P., 1999. Evidence for a Warm Last Glacial Maximum in
1289 the Nordic Seas or an example of shortcomings in UK37'and UK37to
1290 estimate low sea surface temperature? *Paleoceanography* 14, 770-776.
- 1291 Rudels, B., Friedrich, H.J., Quadfasel, D., 1999. The Arctic circumpolar boundary
1292 current. *Deep Sea Research Part II: Topical Studies in Oceanography* 46,
1293 1023-1062.
- 1294 Rudels, B., Meyer, R., Fahrbach, E., Ivanov, V., Østerhus, S., Quadfasel, D., Schauer,
1295 U., Tverberg, V., Woodgate, R., 2000. Water mass distribution in Fram Strait
1296 and over the Yermak Plateau in summer 1997, *Annales Geophysicae*.
1297 Springer, pp. 687-705.
- 1298 Rudels, B., Björk, G., Nilsson, J., Winsor, P., Lake, I., Nohr, C., 2005. The
1299 interaction between waters from the Arctic Ocean and the Nordic Seas north
1300 of Fram Strait and along the East Greenland Current: results from the Arctic
1301 Ocean-02 Oden expedition. *Journal of Marine Systems* 55, 1-30.
- 1302 Sarnthein, M., Jansen, E., Weinelt, M., Arnold, M., Duplessy, J.C., Erlenkeuser, H.,
1303 Flatøy, A., Johannessen, G., Johannessen, T., Jung, S., 1995. Variations in

- 1304 Atlantic surface ocean paleoceanography, 50°- 80° N: A time- slice record
1305 of the last 30,000 years. *Paleoceanography* 10, 1063-1094.
- 1306 Sarnthein, M., Pflaumann, U., Weinelt, M., 2003. Past extent of sea ice in the
1307 northern North Atlantic inferred from foraminiferal paleotemperature
1308 estimates. *Paleoceanography* 18 (2), 1047.
- 1309 Schauer, U., 2004. Arctic warming through the Fram Strait: Oceanic heat transport
1310 from 3 years of measurements. *Journal of Geophysical Research* 109.
- 1311 Schauer, U., Beszczynska-Möller, A., Walczowski, W., Fahrbach, E., Piechura, J.,
1312 Hansen, E., 2008. Variation of measured heat flow through the Fram Strait
1313 between 1997 and 2006, Arctic–Subarctic Ocean Fluxes. Springer, pp. 65-85.
- 1314 Sejrup, H.P., Seppä, H., McKay, N.P., Kaufman, D.S., Geirsdóttir, Á., de Vernal, A.,
1315 Renssen, H., Husum, K., Jennings, A., Andrews, J.T., 2016. North Atlantic-
1316 Fennoscandian Holocene climate trends and mechanisms. *Quaternary*
1317 *Science Reviews* 147, 365-378.
- 1318 Skogseth, R., Haugan, P.M., Jakobsson, M., 2005. Watermass transformations in
1319 Storfjorden. *Continental Shelf Research* 25, 667-695.
- 1320 Ślubowska, M.A., Koç, N., Rasmussen, T.L., Klitgaard-Kristensen, D., 2005.
1321 Changes in the flow of Atlantic water into the Arctic Ocean since the last
1322 deglaciation: Evidence from the northern Svalbard continental margin, 80°N.
1323 *Paleoceanography* 20, PA4014.
- 1324 Ślubowska-Woldengen, M., Rasmussen, T.L., Koç, N., Klitgaard-Kristensen, D.,
1325 Nilsen, F., Solheim, A., 2007. Advection of Atlantic Water to the western and
1326 northern Svalbard shelf since 17,500 cal. yr BP. *Quaternary Science Reviews*
1327 26, 463-478.
- 1328 Ślubowska-Woldengen, M., Koç, N., Rasmussen, T.L., Klitgaard-Kristensen, D.,
1329 Hald, M., Jennings, A.E., 2008. Time-slice reconstructions of ocean
1330 circulation changes on the continental shelf in the Nordic and Barents Seas

- 1331 during the last 16,000 cal. yr BP. *Quaternary Science Reviews* 27, 1476-
1332 1492.
- 1333 Solignac, S., de Vernal, A., Hillaire-Marcel, C., 2004. Holocene sea-surface
1334 conditions in the North Atlantic—contrasted trends and regimes in the
1335 western and eastern sectors (Labrador Sea vs. Iceland Basin). *Quaternary*
1336 *Science Reviews* 23, 319-334.
- 1337 Spielhagen, R.F., Werner, K., Sørensen, S.A., Zamelczyk, K., Kandiano, E., Budeus,
1338 G., Husum, K., Marchitto, T.M., Hald, M., 2011. Enhanced modern heat
1339 transfer to the Arctic by warm Atlantic water. *Science* 331, 450-453.
- 1340 Spielhagen, R.F., Müller, J., Wagner, A., Werner, K., Lohmann, G., Prange, M.,
1341 Stein, R., 2014. Holocene Environmental Variability in the Arctic Gateway.
1342 In: Schulz, M. and Paul, A. (eds.), *Integrated Analysis of Interglacial Climate*
1343 *Dynamics*, Springer Briefs, Springer-Verlag, Berlin, 37-41.
- 1344 Stanford, J., Rohling, E.J., Bacon, S., Roberts, A., Grousset, F., Bolshaw, M., 2011.
1345 A new concept for the paleoceanographic evolution of Heinrich event 1 in the
1346 North Atlantic. *Quaternary Science Reviews* 30, 1047-1066.
- 1347 Stein, R., Fahl, K., 1997. Scientific cruise report of the Arctic expedition ARK-XIII/2
1348 of RV "Polarstern" in 1997= Wissenschaftlicher Fahrtbericht über die Arktis-
1349 Expedition ARK-XIII/2 von 1997 mit FS "Polarstern". *Berichte zur*
1350 *Polarforschung (Reports on Polar Research)* 255.
- 1351 Stern, J. V., Lisiecki, L.E., 2014. Termination 1 timing in radiocarbon dated regional
1352 benthic $\delta^{18}\text{O}$ stacks. *Paleoceanography* 29: 1127–1142.
- 1353 Stockmarr, J., 1971. Tablets with spores used in absolute pollen analysis. *Pollen*
1354 *spores* 13, 615-621.
- 1355 Streel, M., Bless, M., 1980. Occurrence and significance of reworked palynomorphs.
1356 *Mededelingen-Rijks Geologische Dienst* 32, 69-80.

- 1357 Stroeven, A.P., Hättestrand, C., Kleman, J., Heyman, J., Fabel, D., Fredin, O.,
1358 Goodfellow, B.W., Harbor, J.M., Jansen, J.D., Olsen, L., 2016. Deglaciation
1359 of Fennoscandia. *Quaternary Science Reviews* 147, 91-121.
- 1360 Tarasov, L., Peltier, W.R., 2005. Arctic freshwater forcing of the Younger Dryas cold
1361 reversal. *Nature* 435, 662-665.
- 1362 Telford, R.J., 2006. Limitations of dinoflagellate cyst transfer functions. *Quaternary*
1363 *Science Reviews* 25, 1375-1382.
- 1364 Telford, R., Birks, H., 2009. Evaluation of transfer functions in spatially structured
1365 environments. *Quaternary Science Reviews* 28, 1309-1316.
- 1366 Telesinski, M.M., Spielhagen, R.F., Bauch, H.A., 2014. Water mass evolution of the
1367 Greenland Sea since lateglacial times. *Climate of the Past* 10, 123–136. Van
1368 Nieuwenhove, N., Baumann, A., Matthiessen, J., Bonnet, S., de Vernal, A.,
1369 2016. Sea surface conditions in the southern Nordic Seas during the
1370 Holocene based on dinoflagellate cyst assemblages. *The Holocene* 26, 722-
1371 735.
- 1372 Voronina, E., Polyak, L., Vernal, A.D., Peyron, O., 2001. Holocene variations of sea-
1373 surface conditions in the southeastern Barents Sea, reconstructed from
1374 dinoflagellate cyst assemblages. *Journal of Quaternary Science* 16, 717-726.
- 1375 Walczowski, W., Piechura, J., Osinski, R., Wiczorek, P., 2005. The West
1376 Spitsbergen Current volume and heat transport from synoptic observations in
1377 summer. *Deep Sea Research Part I: Oceanographic Research Papers* 52,
1378 1374-1391.
- 1379 Walczowski, W., Piechura, J., 2007. Pathways of the Greenland Sea warming.
1380 *Geophysical Research Letters* 34.
- 1381 Walker, M.J.C., Berkelhammer, M., Björck, S., Cwynar, L.C., Fisher, D.A., Long,
1382 A.J., Lowe, J.J., Newnham, R.M., Rasmussen, S.O., Weiss, H., 2012. Formal
1383 subdivision of the Holocene Series/Epoch: a Discussion Paper by a Working

- 1384 Group of INTIMATE (Integration of ice-core, marine and terrestrial records)
1385 and the Subcommission on Quaternary Stratigraphy (International
1386 Commission on Stratigraphy). *Journal of Quaternary Science* 27, 649-659.
- 1387 Weinelt, M., Sarnthein, M., Pflaumann, U., Schulz, H., Jung, S., Erlenkeuser, H.,
1388 1996. Ice-free Nordic seas during the last glacial maximum. Potential sites of
1389 deepwater formation. *Paleoclimates* 1, 283-309.
- 1390 Weinelt, M., Vogelsang, E., Kucera, M., Pflaumann, U., Sarnthein, M., Voelker, A.,
1391 Erlenkeuser, H., Malmgren, B.A., 2003. Variability of North Atlantic heat
1392 transfer during MIS 2. *Paleoceanography* 18 (3), 1071.
- 1393 Werner, K., Spielhagen, R.F., Bauch, D., Hass, H.C., Kandiano, E., Zamelczyk, K.,
1394 2011. Atlantic Water advection to the eastern Fram Strait — Multiproxy
1395 evidence for late Holocene variability. *Palaeogeography, Palaeoclimatology,*
1396 *Palaeoecology* 308, 264-276.
- 1397 Werner, K., Spielhagen, R.F., Bauch, D., Hass, H.C., Kandiano, E., 2013. Atlantic
1398 Water advection versus sea-ice advances in the eastern Fram Strait during the
1399 last 9 ka: Multiproxy evidence for a two-phase Holocene. *Paleoceanography*
1400 28, 283-295.
- 1401 Werner, K., Müller, J., Husum, K., Spielhagen, R.F., Kandiano, E.S., Polyak, L.,
1402 2016. Holocene sea subsurface and surface water masses in the Fram Strait –
1403 Comparisons of temperature and sea-ice reconstructions. *Quat. Sci. Rev.* 147,
1404 194-209. doi:10.1016/j.quascirev.2015.09.007
- 1405 Williams, G.L., Brideaux, W.W., 1975. Palynologic analyses of Upper Mesozoic and
1406 Cenozoic rocks of the Grand Banks, Atlantic continental margin. Department
1407 of Energy, Mines and Resources: available from Information Canada.
- 1408 Xiao, X., Fahl, K., Müller, J., Stein, R., 2015. Sea-ice distribution in the modern
1409 Arctic Ocean: biomarker records from trans-Arctic Ocean surface sediments.
1410 *Geochimica et Cosmochimica Acta* 155, 16-29.

- 1411 Zamelczyk, K., Rasmussen, T.L., Husum, K., Haflidason, H., de Vernal, A., Ravna,
1412 E.K., Hald, M., Hillaire-Marcel, C., 2012. Paleoceanographic changes and
1413 calcium carbonate dissolution in the central Fram Strait during the last 20ka.
1414 *Quaternary Research* 78, 405-416.
- 1415 Zamelczyk, K., Rasmussen, T.L., Husum, K., Godtlielsen, F., Hald, M., 2014.
1416 Surface water conditions and calcium carbonate preservation in the Fram
1417 Strait during marine isotope stage 2, 28.8-15.4 kyr. *Paleoceanography* 29, 1-
1418 12.
- 1419 Zumaque, J., Eynaud, F., de Vernal, A., 2017. Holocene paleoceanography of the Bay
1420 of Biscay: Evidence for west-east linkages in the North Atlantic based on
1421 dinocyst data. *Palaeogeography, Palaeoclimatology, Palaeoecology* 468, 403-
1422 413.

Core name	Abbreviation used in text	Core location	Latitude	Longitude	Water depth (m)	Core length (cm)	Modern sea-surface conditions			Core sampling	
							SST in summer (°C)	SSS in summer (psu)	Sea-ice cover (month/yr)	Length (cm)	Interval (cm)
MSM5/5-712-2	MSM5-712	Western Svalbard margin	78°54.937'N	06°46.036'E	1,487	950	4.94±1.40	34.73±0.43	1.2±1.7	10-283	4
										283-777	8
PS2863-1	PS2863	NW Svalbard margin	80°33.46'N	10°17.96'E	808	580	2.3±2.3	33.3±0.9	9.32±2.0	41-184	4
PS2863-2			80°33.47'N	10°17.93'E	807	41				0-39	1

Table 1. Information on the study cores

Core location, water depth (m) and recovery (cm); present day sea-surface conditions at the core sites (Conkright et al., 2002) and sea-ice cover from NSIDC. Sections and subsampling intervals (cm) are indicated.

Table 2. Radiocarbon chronology of cores MSM5-712, PS2863-1 and PS2837-5

Core	Depth (cm)	Conventional ¹⁴ C age (¹⁴ C years BP)	Calibrated age (cal. years BP)	Minimum age	Maximum age	Lab n°	Reference
MSM5-712	10-12	815 ± 25	381.7	218	471.4	KIA 45217	Werner et al., 2013
MSM5-712	20-22	1,570 ± 25	1,018.7	884	1,161.2	KIA 41024	Werner et al., 2013
MSM5-712	27-29	1,985 ± 25	1,432.2	1,299.7	1,568.6	KIA 45218	Werner et al., 2013
MSM5-712	40-42	2,565 ± 25	2,114.1	1,935.9	2,284	KIA 45219	Werner et al., 2013
MSM5-712	60.5	3,365 ± 30	3,093.8	2,896	3,295.1	SacA 19113	Giraudeau (in preparation)
MSM5-712	94.5	4,915 ± 30	5,077.5	4,861.2	5,264.5	SacA 19114	Giraudeau (in preparation)
MSM5-712	139	6,440 ± 30	6,796.2	6,622.9	6,960.5	SacA 19115	Giraudeau (in preparation)
MSM5-712	169	7,305 ± 35	7,669.5	7,530.1	7,809.3	KIA 38080	Werner et al., 2013
MSM5-712	192	7,815 ± 45	8,194.9	8,029.8	8,342.9	KIA 41025	Werner et al., 2013
MSM5-712	214.5	8,362 ± 50	8,730.4	8,526.8	8,937.4	Poz-30723	Aagaard-Sørensen et al., 2014a
MSM5-712	280.5	9,220 ± 50	9,895.3	9,640.2	10,137.6	KIA 37423	Aagaard-Sørensen et al., 2014a
MSM5-712	322.5	9,580 ± 47	10,699.2	10,324.1	11,203.5	Poz-30725	Aagaard-Sørensen et al., 2014a
MSM5-712	350	10,940 ± 50*	12,047.8	11,375.4	12,443.1	KIA 7571	Nørgaard-Pedersen et al., 2003
MSM5-712	428-431	12,358 ± 63	13,920.4	13,737.9	14,137.5	Poz-30726	Aagaard-Sørensen et al., 2014a
MSM5-712	480	12,655 ± 60*	14,077.5	13,892.8	14,296.8	KIA	Nørgaard-Pedersen et

						7572	al., 2003
MSM5-712	660	12,9400 ± 70*	14,792.5	14,450	15,620	KIA-10864	Nørgaard-Pedersen et al., 2003
MSM5-712	687.5	14,650 ± 75	17,052.9	16,555.4	17,465.1	Poz-30727	Zamelczyk et al., 2014
MSM5-712	716.25	17,200 ± 120	19,912.5	19,337.2	20,379.1	Poz-38427	Zamelczyk et al., 2014
MSM5-712	762.25	19,300 ± 140	22,444.5	21,856.3	22,841.4	Poz-30728	Zamelczyk et al., 2014
MSM5-712	801	20,150 ± 130**	23,669.9	23,237	24,059.6	-	Jessen et al., 2010
MSM5-712	842	20,580 ± 130**	24,972.2	24,285.4	25,628.1	-	Jessen et al., 2010
MSM5-712	876	23,340 ± 200**	27,068.9	26,339.5	27,562	-	Jessen et al., 2010
MSM5-712	882.75	24,480 ± 190	27,521.8	26,659.1	27,944.5	Poz-30729	Zamelczyk et al., 2014
PS2863-1	36-39	7,150 ± 35	7,537.3	7,319	7,7717.3	OS-122305	This study
PS2863-1	52-54	9,336 ± 40	10,156.1	9,841.2	10,508.4	KIA-50537	This study
PS2863-1	120	12,840 ± 150**	14,700.4	14,250.5	15,122.9	-	Jessen et al., 2010
PS2863-1	133	13,140 ± 150**	14,985.6	14,521.4	15,397.6	-	Jessen et al., 2010
PS2863-1	162.5	15,660 ± 80	18,387.8	17,883.2	18,814.8	KIA-50401	This study
PS2863-1	168.5	17,700 ± 100	19,669.8	18,896.3	20,522.2	KIA-50402	This study
PS2863-1	199.5	19,140 ± 120	22,643.5	22,074.2	23,223.2	KIA-50403	This study
PS2837-5	10.5	535 ± 25	1,46.7	11.1	270.4	KIA-7570	Nørgaard-Pedersen et al., 2003
PS2837-5	50.5	2,130 ± 40	1,639.3	1,451.7	1,847.8	KIA-4652	Nørgaard-Pedersen et al., 2003

PS2837-5	76.5	3,340 ± 35	3,059.3	2,858.5	3,268.7	KIA 8927	Nørgaard-Pedersen et al., 2003
PS2837-5	111.5	4,965 ± 45	5,153.4	4,908.1	5,392.3	KIA 8928	Nørgaard-Pedersen et al., 2003
PS2837-5	153.5	7,405 ± 45	7,709	7,483.3	7,874.6	KIA 8929	Nørgaard-Pedersen et al., 2003
PS2837-5	182.5	8,070 ± 60	8,506.1	8,322.7	8,780	KIA 4653	Nørgaard-Pedersen et al., 2003
PS2837-5	225.5	9,290 ± 60	10,009.9	9,823.6	10,499.3	KIA 8930	Nørgaard-Pedersen et al., 2003
PS2837-5	253.5	10,940 ± 50	12,243.5	11,886	12,354.8	KIA 7571	Nørgaard-Pedersen et al., 2003
PS2837-5	274.5	12,155 ± 60	13,411	13,151.6	13,620	KIA 10863	Nørgaard-Pedersen et al., 2003
PS2837-5	300.5	12,+655 ± 60	14,195.7	13,972.5	14,541.8	KIA 7572	Nørgaard-Pedersen et al., 2003
PS2837-5	359.5	12,940 ± 70	14,746	14,466.5	15,080.7	KIA 10864	Nørgaard-Pedersen et al., 2003
PS2837-5	382.5	16,040 ± 80	18,593.1	18,001.1	19,025.9	KIA 10865	Nørgaard-Pedersen et al., 2003
PS2837-5	389.5	17,440 ± 110	20,123.8	19,543.2	20,639.3	KIA 4654	Nørgaard-Pedersen et al., 2003
PS2837-5	415.5	24,230 ± 180	27,504.8	26,553.3	28,243.1	KIA 7573	Nørgaard-Pedersen et al., 2003

All ¹⁴C dates are from *Neogloboquadrina pachyderma* (sinistral). The calibrated ages correspond to the modelled weighted mean age obtained after 8000 iterations executed with the Bacon 2.2 software (see text section 4).

* Ages obtained from a correlation with core PS2837-5

** Ages obtained from a correlation with the western Svalbard MS stack

Figure captions

Fig. 1 Map of the main surface currents in the Fram Strait and around Svalbard and location of the study sites MSM5/5-712 and PS2863 (yellow stars). Limits of minimum (September) and maximum (March) median sea-ice cover extent from 1979 to 2016 are represented by blue and gray dotted lines, respectively, obtained from the Sea Ice Index (Fetterer et al., 2016). Red arrows indicate warmer Atlantic waters derived from the North Atlantic Drift and were reproduced with respect to Walczowski et al. (2005). Blue arrows indicate cold surface water currents. In the Svalbard close-up, the Arctic Coastal Front and the Polar Front are depicted, shown by a dotted and a uniform black line, respectively. Locations of other cores discussed in the text are indicated by black dots. Main features of the sea-floor such as the Yermak Plateau (YP), the Storfjorden and the Mohn and Knipovich ridges are also indicated on the map. EGC: East Greenland Current, WSC: West Spitsbergen Current, NwASC: Norwegian Atlantic Slope Current, NwAC: Norwegian Atlantic Current, ESC: East Spitsbergen Current, SCC: South Cape Current, RAC: Return Atlantic Current, SB: Svalbard Branch, YB: Yermak Branch

Fig. 2 Age model of cores MSM5-712, PS2863-1 and PS2837-5 obtained by using the Bacon 2.2 software (Blaauw and Christen, 2011) (see Table 2 for data and text section 4). The red line corresponds to the weighted average. Gray areas show the most probable ages based on Bayesian statistics with default probability intervals of 95% (2-sigma). The dates are indicated in yellow and the correlated tie points are indicated in blue, with numbering as follows : (1) correlations with core PS2837-5 based on total organic carbon (cf. Müller and Stein, 2014), (2) correlations with the western Svalbard magnetic susceptibility stack of Jessen et al. (2010) from Müller and Stein (2014), (3) sedimentological correlation with core PS2837-5 based on IRD (this study; see triangle and dotted lines), (4) correlation of a fine-grained layer in core

PS2863-1 with the rapidly deposited layer in the western Svalbard (Jessen et al., 2010). The vertical shaded zone corresponds to the interval of the rapidly deposited sediment layer defined by Jessen et al. (2010), including its 95% probability. Since the rapid sedimentation rate event is well-documented regionally (Jessen et al., 2010; Lucchi et al., 2015), we added hiatuses at the depths of the first and last age of the event, so the model would interpret the accumulation rate of this interval separately.

Fig. 3 Palynomorph concentrations at sites PS2863 and MSM5-712. The errors of dinocyst concentrations are illustrated by a gray shading. Dinocyst fluxes are represented by a dotted thick line.

Fig. 4 Percentages of dinocyst taxa at site MSM5-712 (in light orange) superimposed on the percentages of dinocyst taxa at site PS2863 (in gray). Zones described in the text are delimited by horizontal dotted lines. The age of the LGM is established according to the MARGO working group (Kucera et al., 2005). The age of the Heinrich Stadial 1 (H1) is determined according to Gibb et al. (2014). Limits of the Bølling-Allerød (BA) and the Younger Dryas (YD) intervals are set according to Rasmussen et al. (2006); the divisions between Early, Mid- and Late Holocene follow suggestions by Walker et al. (2012). On the calibrated age axis, the black bar indicates the interval of the rapidly deposited sediment layer described by Jessen et al. (2010), including its 95% probability.

Fig. 5 Light micrographs and SEM photographs of the morphological variations of *Spiniferites ramosus* and *Nematosphaeropsis labyrinthus* in sediments of the 14.3-11.4 ka interval in cores PS2863-1 and MSM5-712.

1-3: Core PS2863-1, slide 3145-6E, 93-94 cm (EF G24/2). *Spiniferites ramosus* with an ovoid to a pear-shaped body. The gonol processes are shorter at the apex than at the antapex.

4-6: Core PS2863-1, slide 3145-6E, 93-94 cm (EF K20/2). *Spiniferites ramosus* with a spherical central body and long radial processes which have an equivalent length all around the cyst body. The specimen exposes long trifurcations and bifurcate tips.

7-8: Core PS2863-1, side 3145-6C, 93-94 cm (EF L16/1). A small specimen of *Spiniferites ramosus* having aberrant morphologic characteristics like the development of an apical boss and a microgranular surface body. The processes are short and their tips are irregular.

9-10: Core PS2863-1, slide 3145-6E, 93-94 cm (EF G23/4). *Nematosphaeropsis labyrinthus* with a spherical body and solid processes. The cyst shows a particularly clear paratabulation.

11-13: Core PS2863-1, slide 3145-6E; 93-94 cm (EF G24/2). A large ovoid specimen of *Spiniferites ramosus* which developed a partial trabecular network.

14-15: Core MSM5-712, slide 2799-6; 410-411 cm (EF H22/1). Specimen of *Spiniferites ramosus* with a spherical body and relatively long trifurcations exposing at least one clear trabecula joining the distal ends of two adjacent processes.

16: Core MSM5-712, slide 2799-6; 410-411 cm (EF H17/3). Another specimen of *Spiniferites ramosus* exposing at least one clear trabecula.

17: Core PS2863-1, sample 3145-5, 89-90 cm. SEM photograph of a *Nematosphaeropsis labyrinthus* specimen with a particularly well-developed paratabulation with large sutural ridges and solid processes.

18-19: Core PS2863-1, sample 3145-5, 89-90 cm. SEM photographs of two different specimens of *Spiniferites ramosus* exposing random processes being connected by a single trabecular liaison, at the cingulum (18) and at the antapex (19).

20: Core PS2863-1, sample 3145-5, 89-90 cm. SEM photograph of a *Spiniferites ramosus* specimen with an almost complete trabecular network.

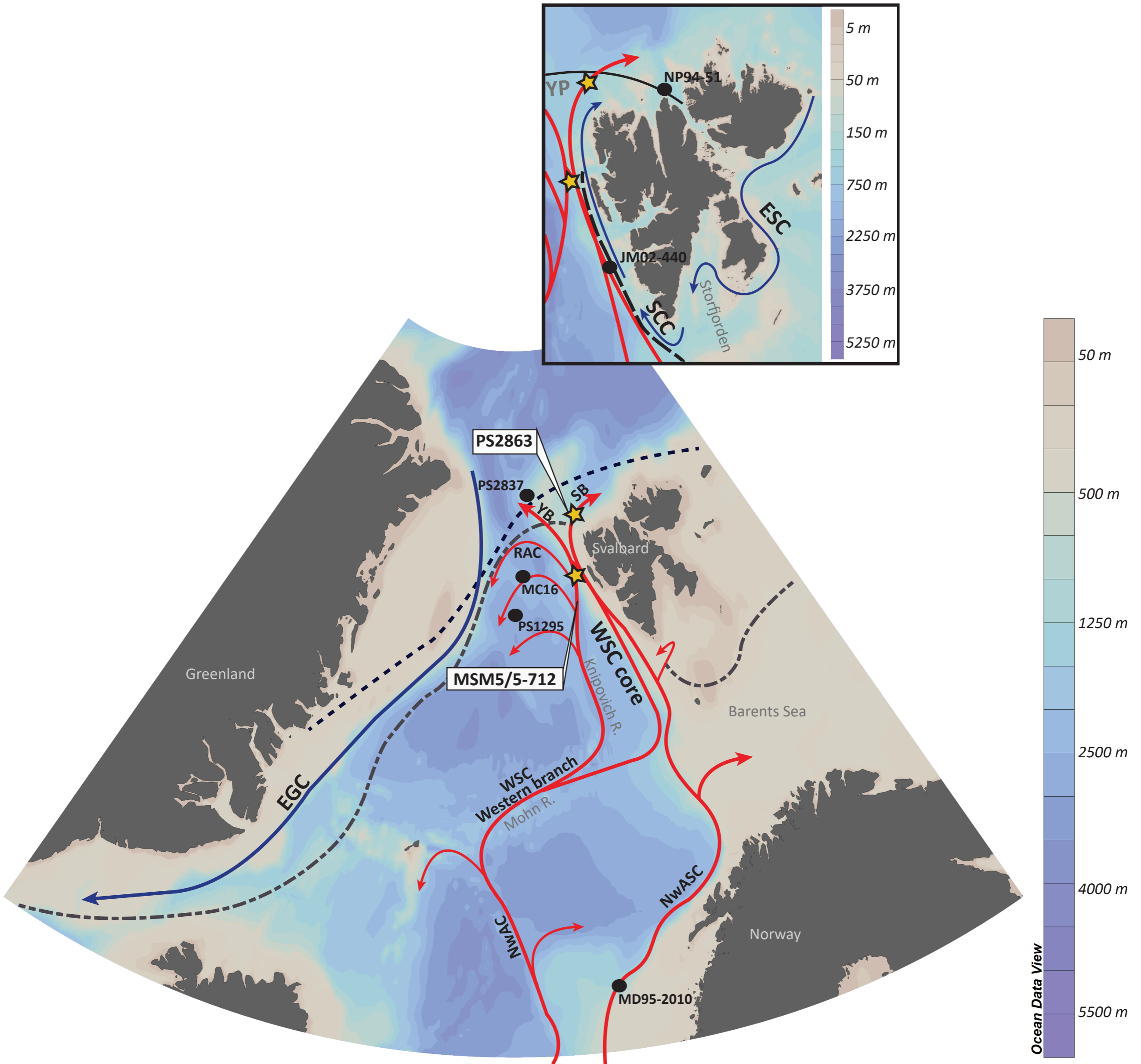
Fig. 6 Reconstructions of sea-surface conditions at site MSM5-712 including (a) summer and winter SSTs in red and blue, respectively, (b) summer and winter SSSs in red and blue, respectively, (c) gray dots indicating samples with at least one colony of *Pediastrum*, (d) sea-ice cover duration, and (e) productivity. Mean values are represented by a thin line, the thick line shows a five-point running average. Maximum and minimum values are represented in brighter shading. In (f) is the distance of the five closest analogs. Black triangles indicate modern values at the core site (SSTs and SSSs in summer) from the World Ocean Atlas 2001 (Conkright et al., 2002) and the average sea-ice cover extent from NSIDC data. Zones as described in the text are divided by horizontal black dotted lines. On the calibrated age axis, the black bar indicates the interval of the rapidly deposited sediment layer as defined by Jessen et al. (2010), including its 95% probability while the gray bar represents the rapidly deposited sediment layer at the site.

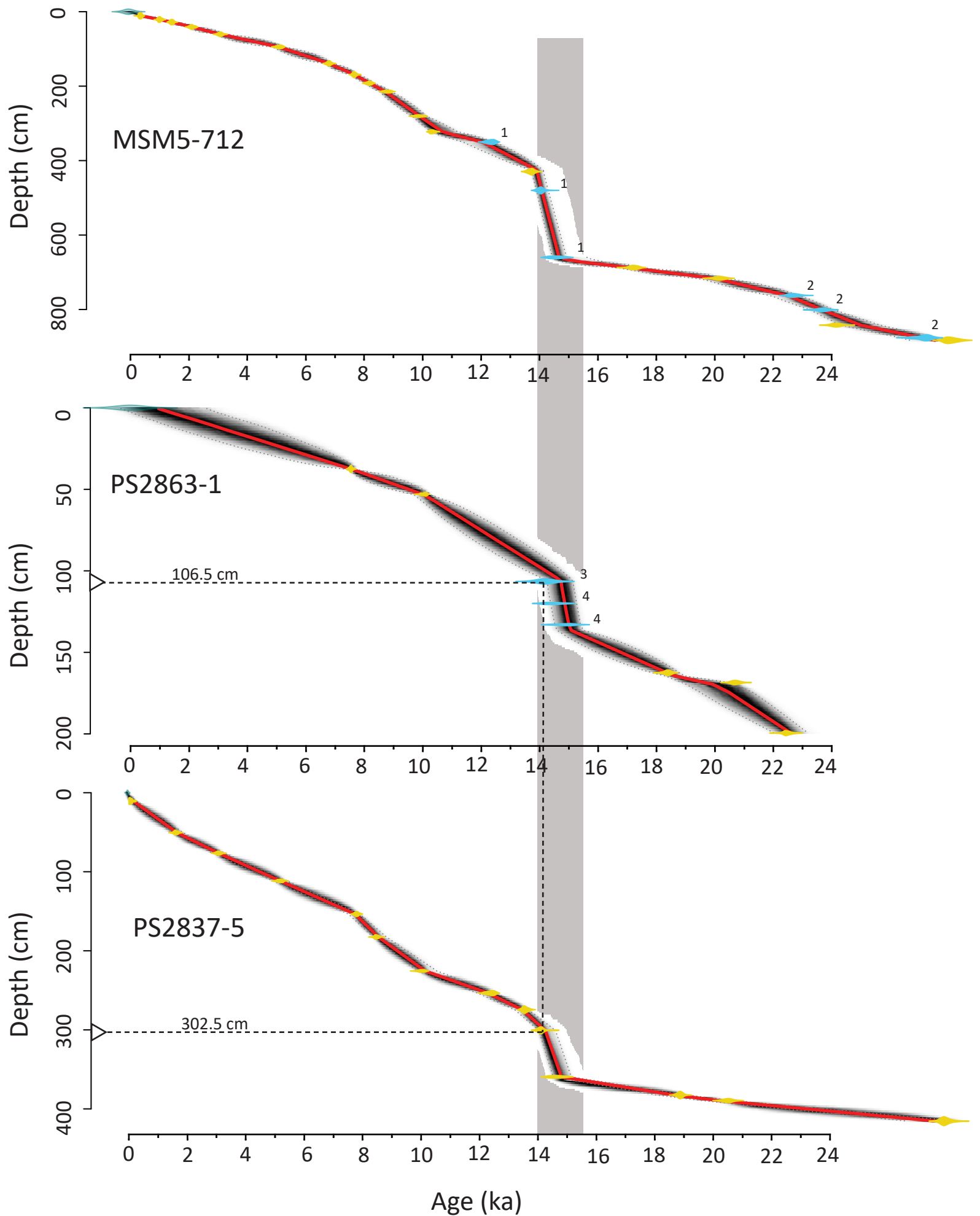
Fig. 7 Close-up of sea-surface conditions at site MSM5-712 during the BA interstadial including (a) summer and winter SSTs in red and blue, respectively, (b) $\delta^{18}\text{O}$ of planktic foraminifer *N. pachyderma* (sinistral) tests in core MD95-2010 in black (Dokken and Jansen, 1999), sea-ice cover proxy $\text{P}_{\text{BIP}_{25}}$ in dark blue (Müller et al., 2012; Müller and Stein, 2014), (c) summer and winter SSSs in red and blue, respectively, (d) occurrence of at least one colony of *Pediastrum* marked by gray dots, (e) sea-ice cover duration, (g) productivity, (h) dinocyst concentrations in light blue in addition to (i-j-k) percentages of three dinocyst taxa relevant in this time interval. The two finer dotted lines indicate the limits of a cooling event (see text section 6.2.2). The vertical gray bar represents the rapidly deposited sediment layer at the site.

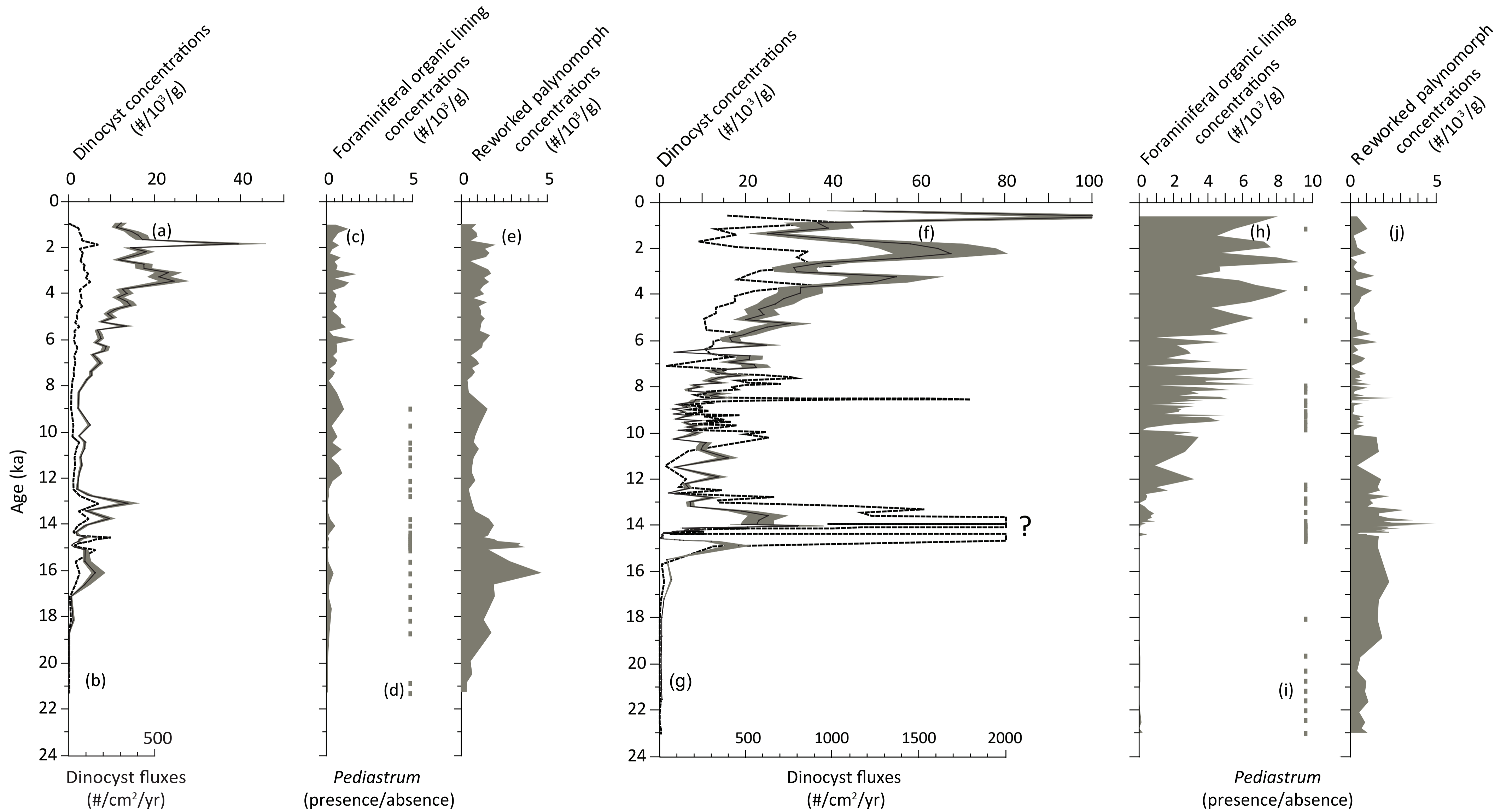
Fig. 8 Reconstructions of sea-surface conditions at site PS2863 including (a) summer and winter SSTs in red and blue, respectively, (b) summer and winter SSSs in red and blue, respectively, (c) gray dots indicating samples with at least one colony of *Pediastrum*, (d) sea-ice cover duration, (e) productivity, and (f) the distance of the five closest analogs. For explanations see Fig. 6.

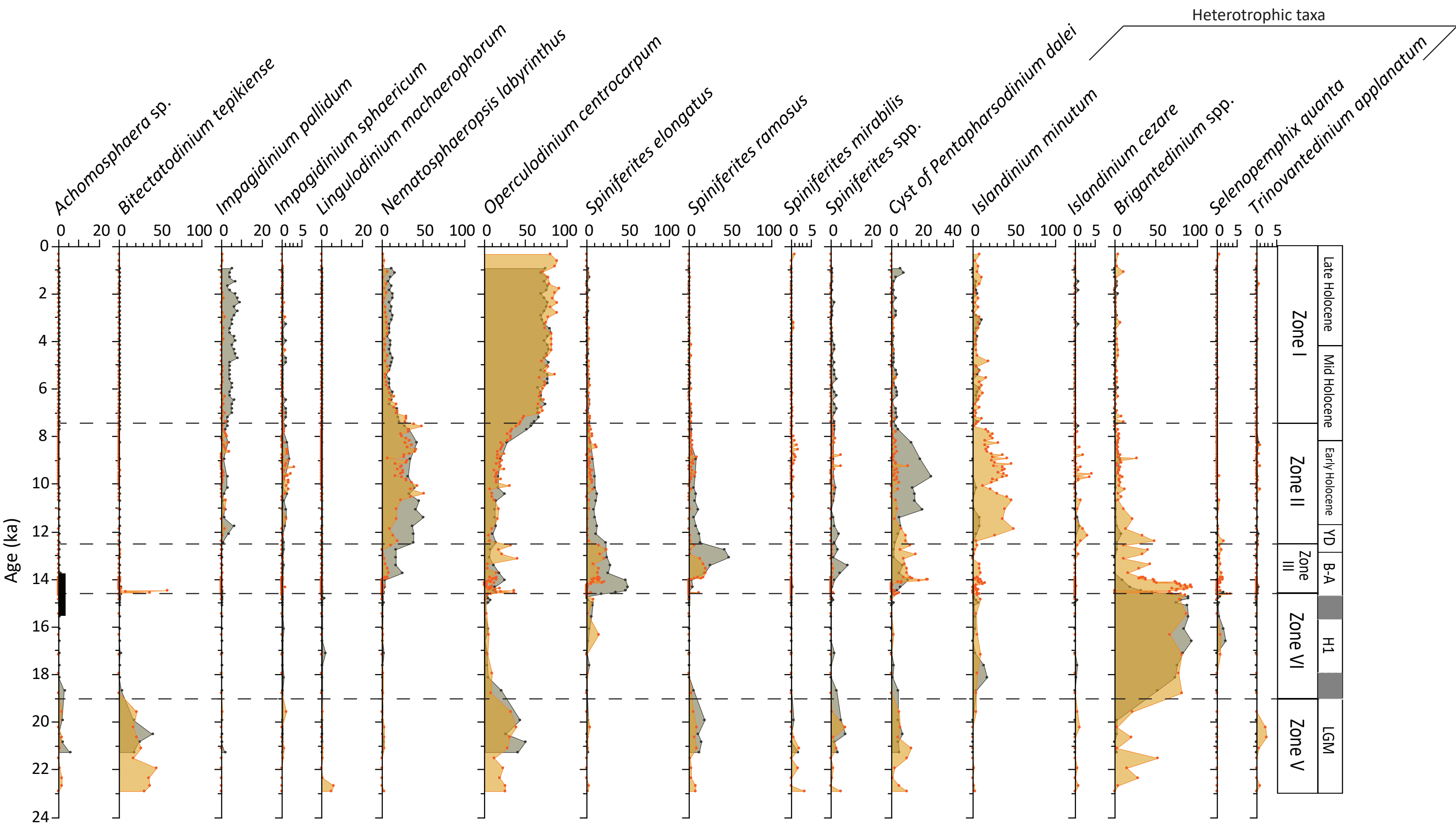
Fig. 9 Reconstructions of sea-surface conditions at site PS2863 (dotted lines) superimposed by the reconstructions of sea-surface conditions at site MSM5-712 (uniform lines) including (a) summer and winter SSTs in red and blue, respectively, (b) summer and winter SSSs in red and blue, respectively, (c) sea-ice cover duration. Only mean values are presented. On the calibrated age axis, the black bar indicates the interval of the rapidly deposited sediment layer as defined by Jessen et al. (2010), including its 95% probability.

Fig. 10 Sea-surface reconstructions at site MSM5-712 including (a) sea-ice cover seasonal duration to be compared with (b) the $P_{BIP_{25}}$ index from Müller et al. (2012) and Müller and Stein (2014) represented by a dark blue line. Data are presented with the chronology described in this paper to permit better correlations with our records. Percentages of heterotrophic taxa (c) *I. minutum* in blue and (d) *Brigantedinium* spp. in purple and percentages of phototrophic taxa (e) *O. centrocarpum* in orange and (f) *B. tepikiense* in yellow. The figure also illustrates (g) SSTs in summer (red) and winter (blue), (h) the $^{231}\text{Pa}/^{230}\text{Th}$ record (green) as a proxy of AMOC strength (McManus et al., 2004), (i) SSSs in summer (red) and winter (blue) and (j) $\delta^{18}\text{O}$ data (gray) from the NGRIP ice core (Andersen et al., 2004b). On the calibrated age axis, the black bar indicates the interval of the rapidly deposited sediment layer defined by Jessen et al. (2010), including its 95% probability.



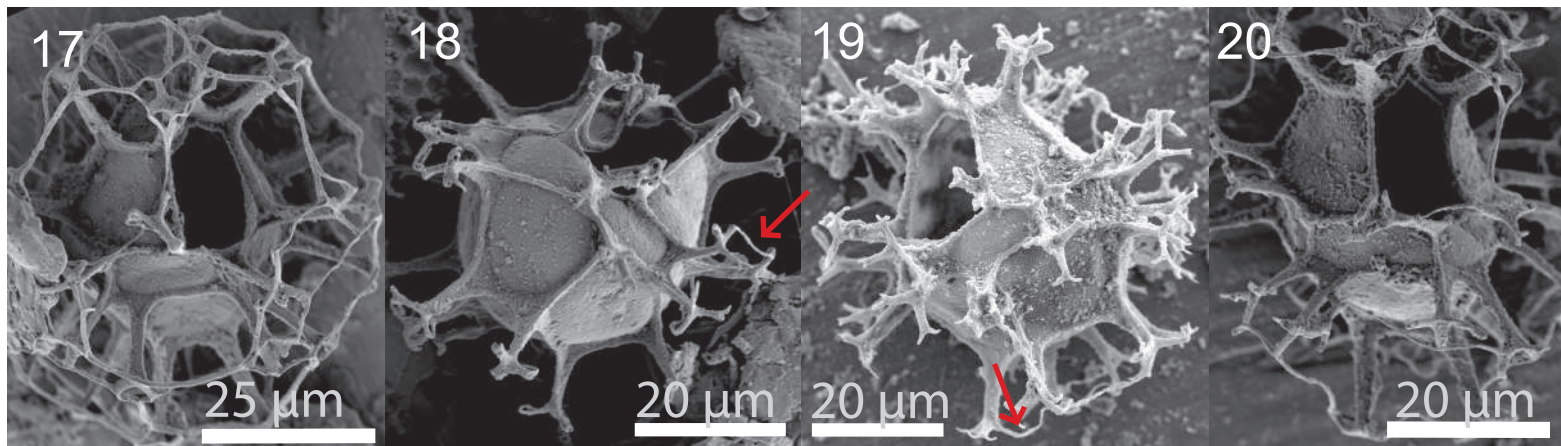
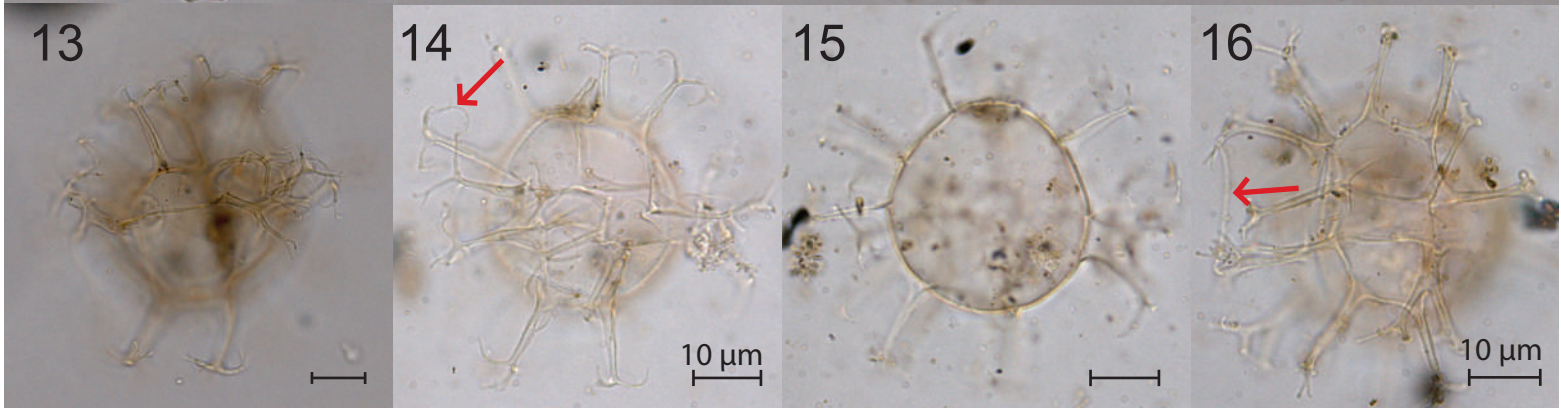
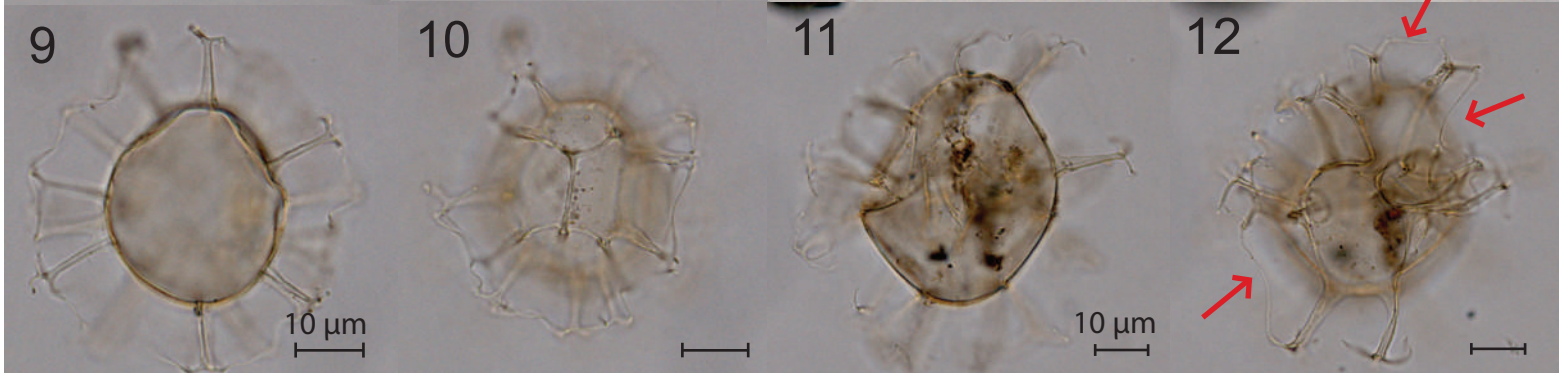


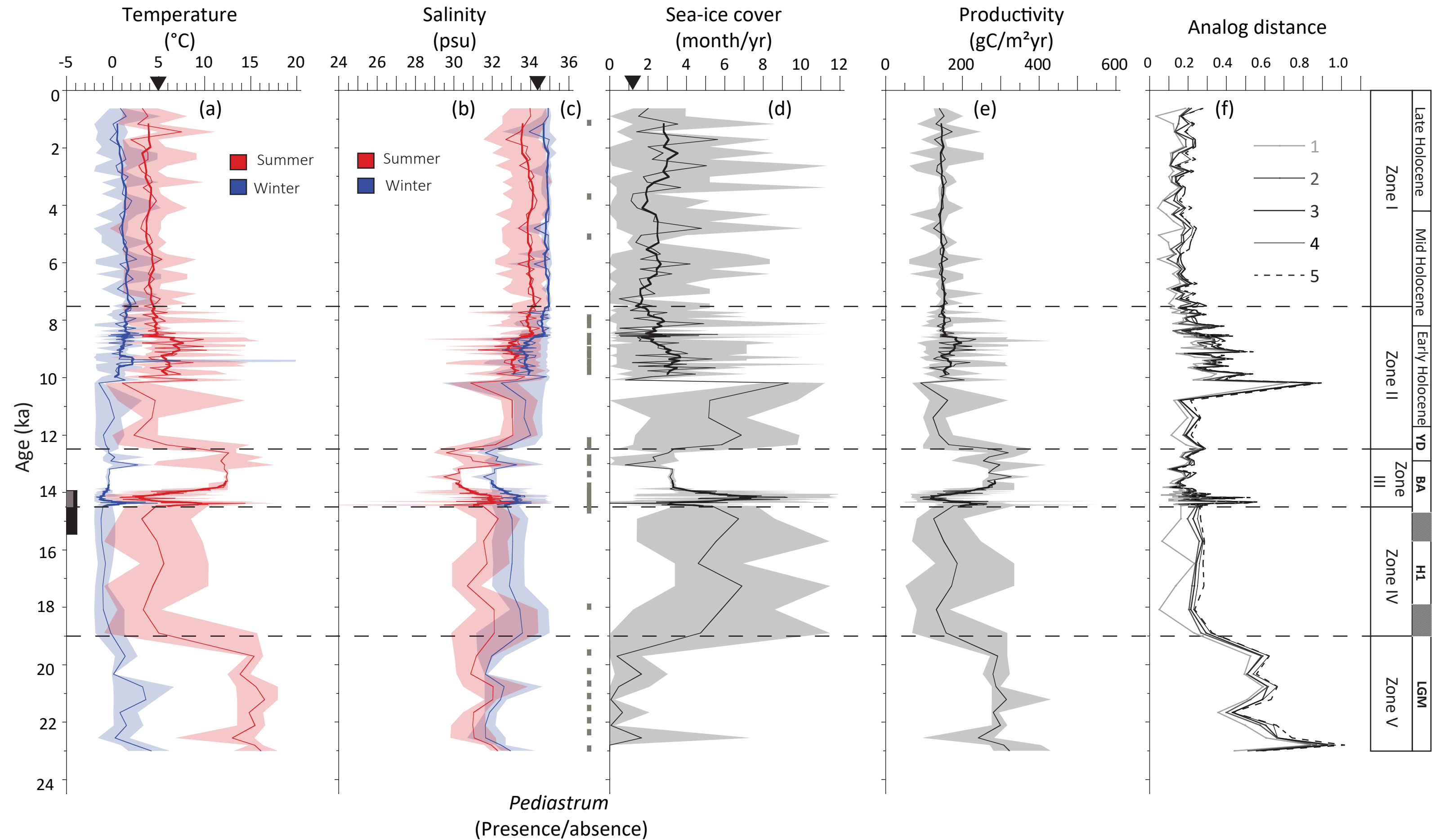


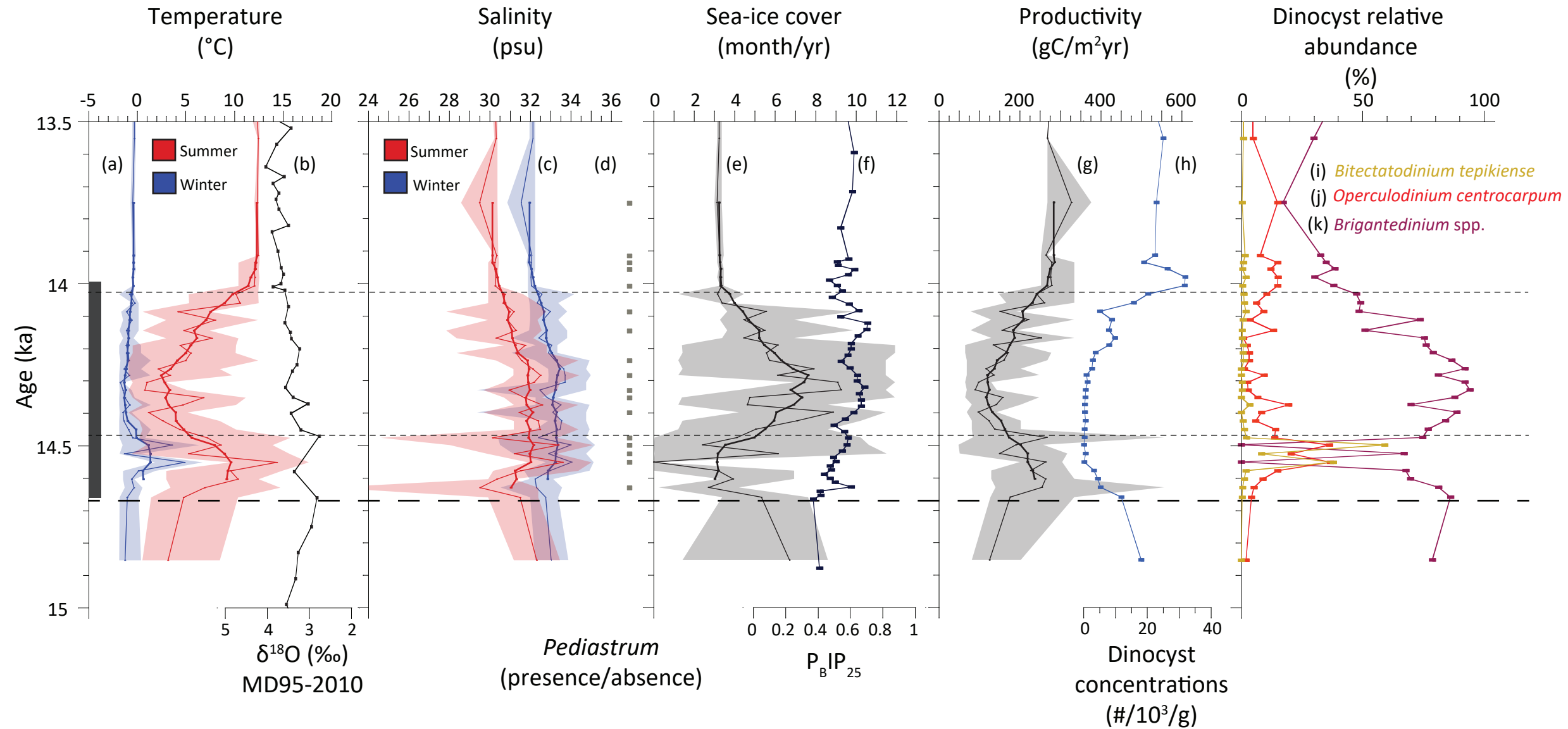


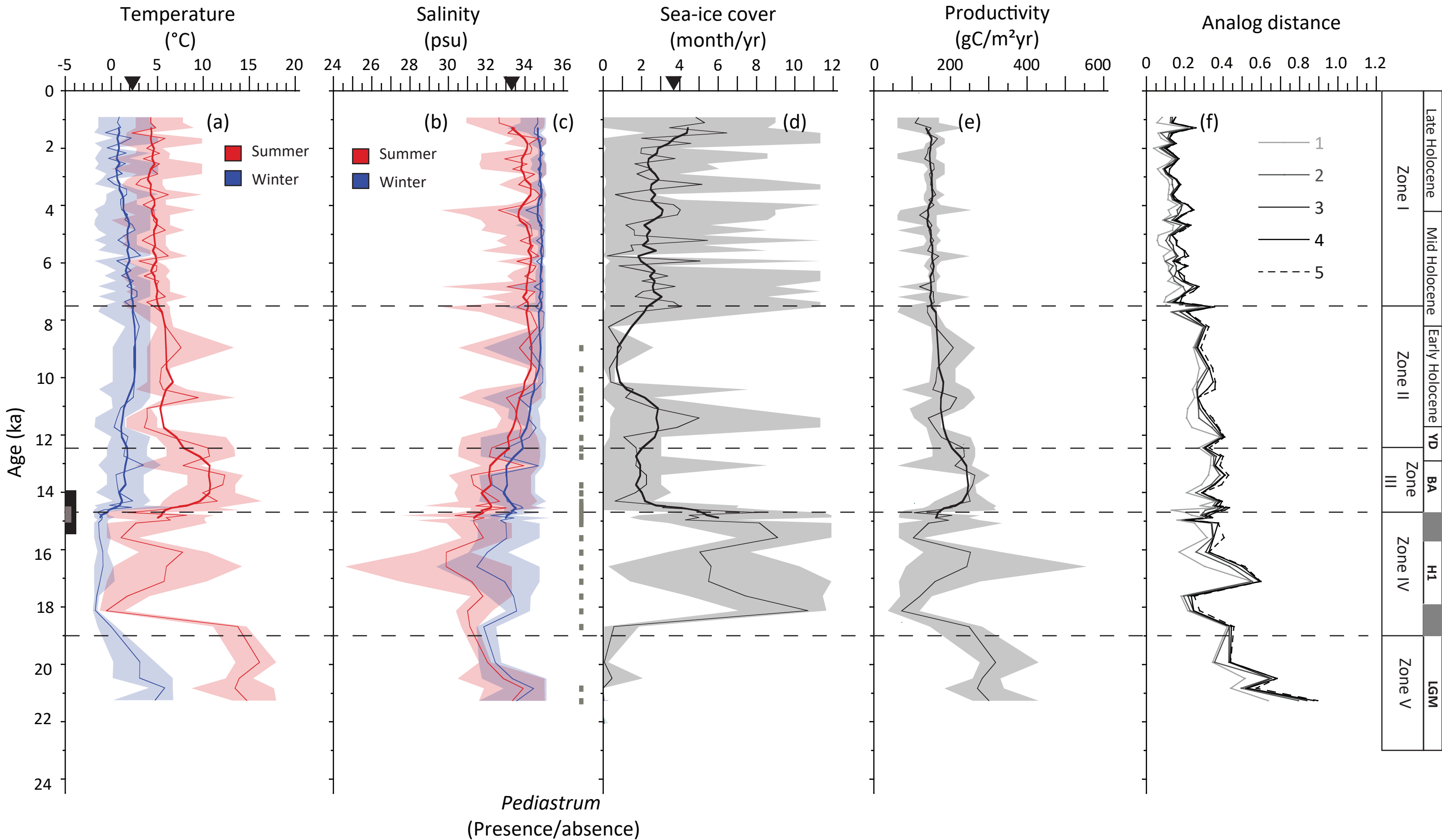
Heterotrophic taxa

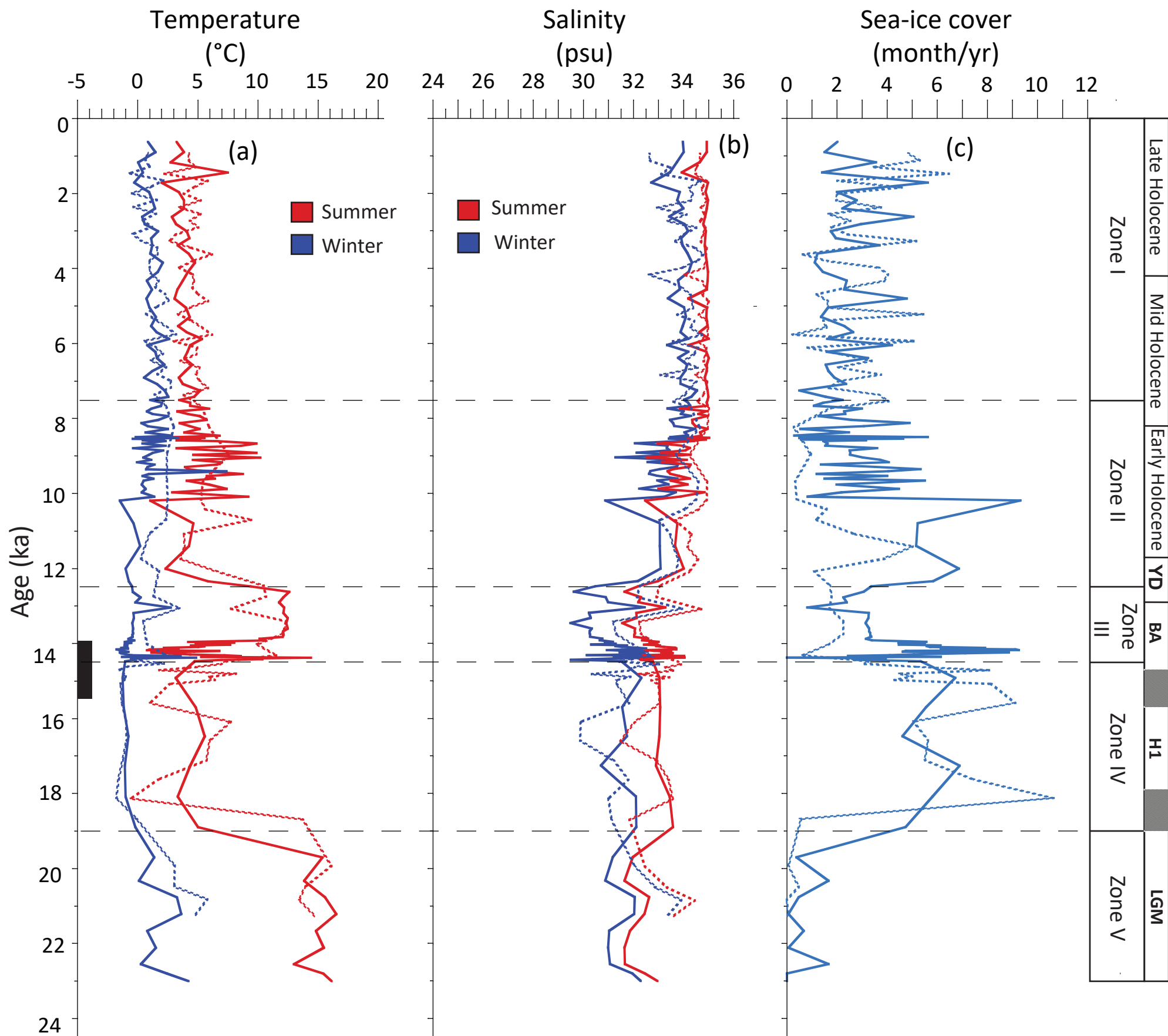
	Late Holocene	Mid Holocene	Early Holocene	YD	B-A	H1	LGM
Zone I							
Zone II							
Zone III							
Zone VI							
Zone V							











Late Holocene	Mid Holocene	Early Holocene	YD	Bølling-Allerød	Heinrich 1	LGM
---------------	--------------	----------------	----	-----------------	------------	-----

